
Subseasonal to interannual variations of sea surface temperature, salinity, oxygen anomaly, and transmissivity in Santa Monica Bay, California from 1987 to 1997

Nikolay P. Nezlin, John J. Oram¹,
Paul M. DiGiacomo² and Nicolas Gruber¹

ABSTRACT - While the basic hydrographic and circulation patterns of Santa Monica Bay (SMB) are relatively well known, the seasonal and interannual variations of these patterns are not well established nor are the mechanisms behind them well understood. We analyzed 10 years of hydrographic observations (1987–1997) in the surface layer of SMB, off southern California, to establish the mean seasonal cycle and to deduce patterns of subseasonal to interannual variability of sea surface temperature, salinity, oxygen anomaly (the difference between oxygen concentration and its solubility), and transmissivity using empirical orthogonal functions and time-lagged cross-correlation methods. All four variables exhibit distinct seasonal variations, whose spatial distributions are a consequence of the interaction of bottom topography, vertical mixing, horizontal advection, freshwater discharge, and biological processes. The seasonal anomalies of all four parameters were estimated by removing the mean seasonal cycle. They exhibit three basic patterns: (1) an inshore/offshore gradient; (2) a balance between horizontal advection of the California Current from the northwest and the Southern California Countercurrent from the south; and (3) freshwater discharge from Ballona Creek. Air/sea heat flux and vertical mixing are the main factors regulating the dynamics of sea surface temperature. Freshwater discharge centered at Ballona Creek is the principal factor creating the salinity pattern. The annual mean oxygen anomaly shows a substantial supersaturation across the entire SMB. The variations of oxygen anomalies are regulated by local biological productivity, vertical mixing, and horizontal transport. Vertical mixing influences water transparency by suspension of sediments and nutrient supply stimulating phytoplankton growth. A remarkably clear pattern of spatio-temporal variations of all parameters is observed in a relatively small basin; these variations are regulated by both

local meteorological factors (air temperature, wind, and atmospheric precipitation) and remote forcing, including the El Niño-Southern Oscillation (ENSO) cycle.

INTRODUCTION

Santa Monica Bay (SMB) is a semi-enclosed bay within the Southern California Bight (SCB) (Figure 1). The bottom topography of the SCB consists of ranges of submarine mountains and valleys and is neither classical continental shelf nor continental slope; Emery (1960) called it the Southern California Borderland. The continental shelf in SMB is wide (>12 km) compared to other parts of the SCB. Two canyons cross the shelf: Santa Monica Canyon, in the northern part of SMB, is a relatively wide trench; while Redondo Canyon, in the southern part, is a narrow trench that almost reaches the shore (Figure 1). The shelf slope is steep, sometimes reaching 14.5° (Emery 1960).

The hydrographic processes in SMB are determined by a complex pattern of surface currents (Lynn and Simpson 1987, Hickey 1992, 1993, Hickey *et al.* 2003). The relatively cold, low-saline, and high-oxygen waters of the southward flowing California Current penetrate to SMB from the northwest through the Santa Barbara Channel. This flow is especially intensive in spring (Dorman and Palmer 1981, Hickey 1993, Bray *et al.* 1999, DiGiacomo and Holt 2001). The relatively warm, salty, and low-oxygen waters of the poleward Southern California Countercurrent (Sverdrup and Fleming 1941) penetrate to the basin alongshore from the southeast through the strait between the San Pedro Peninsula and Santa Catalina Island. Poleward flow within SCB exhibits significant seasonal variations.

¹University of California Los Angeles, Los Angeles, CA 90095-8357

²Jet Propulsion Laboratory, California Institute of Technology, Pasadena, CA 91109-8099

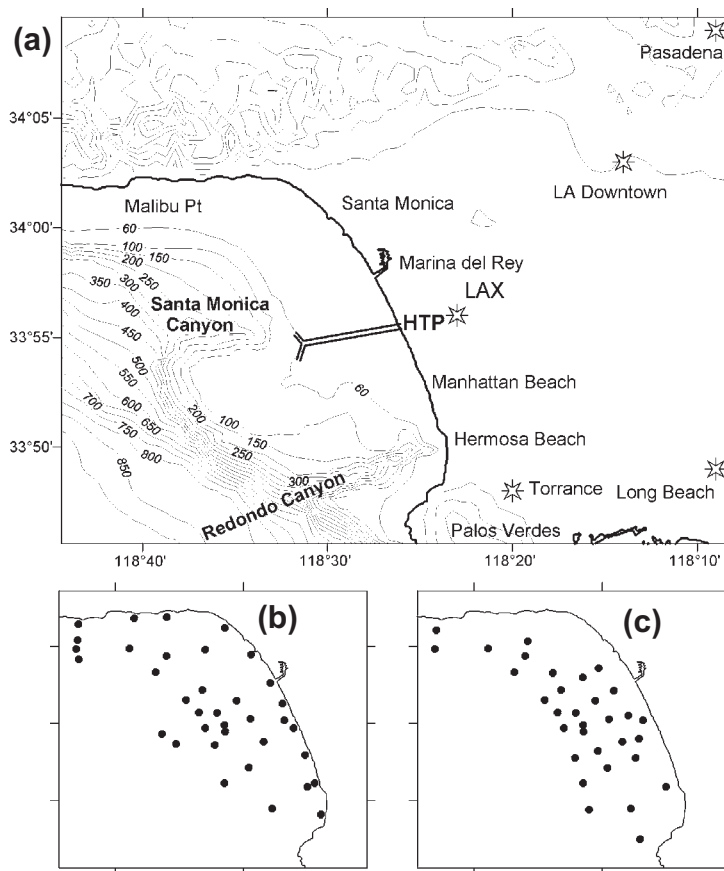


Figure 1. (a) Bottom topography of the Santa Monica Bay and location of meteorological stations where air temperature and precipitation were measured. Isolines indicate bottom depth and land elevation (m). (b), and (c) Maps of hydrographic stations surveyed in September 1987-June 1994 and September 1994-December 1997, respectively. See Table 1 and 2 for exact station locations.

Maximum poleward flow occurs in summer or early fall, and is also intensive in winter; minimum equatorward flow occurs during spring (Hickey 1979, 1993). The seasonal mean flow is equatorward during fall and winter in the narrow inshore shelf zone of SMB (Hickey 1992). The temperature gradients near the coast are enhanced by the effects of local wind-driven upwelling, resulting from alongshore equatorward wind typical for this geographical zone (Bakun and Nelson 1991). Wind over SMB is relatively weak because it is sheltered from the north by a coastal mountain range (Dorman and Winant 1995).

The vertical stratification of the water column is strong as a consequence of intensive surface heating and low vertical mixing due to the low wind stress in this comparatively protected area (Hickey 1992).

This strong stratification is only intermittently broken in late winter/early spring when individual wind events can lead to local upwelling (Gruber *et al.* in preparation). Current fluctuations over the inner SMB shelf have significant short-period variance; these fluctuations appear to be driven predominantly by boundary forcing of the outer shelf and only secondarily by local wind stress (Winant and Bratkovich 1981, Hickey 1992, Hickey *et al.* 2003). SMB is an area of active mesoscale eddy dynamics. Cyclonic eddies of <50 km diameter (often <10 km) are especially numerous in fall and winter (DiGiacomo and Holt 2001).

In contrast to open oceanic regions, freshwater discharge plays a very important role in determining the hydrographic, chemical, and biological state of coastal waters. While freshwater discharge to SMB is small compared to other coastal regions, its influence on coastal water after rainstorms can be substantial. Such storm events are of particular interest as they are often associated with the transport of pollutants from the land into the coastal seas (Dwight *et al.* 2002, Ackerman and Weisberg 2003). The freshwater discharge to SMB is relatively small but comes from a variety of sources. The rainwater flows to SMB through small storm drains and two small rivers: Malibu Creek, which discharges near Malibu Point; and Ballona Creek, whose mouth is located near Marina del Rey. The watershed of

Ballona Creek occupies the majority of the coastal plain, with an area of about 350 km². Ballona Creek is lined with concrete to speed the water flow to the ocean, resulting in runoff that is linearly related to rainfall (Ackerman and Weisberg 2003). Annual mean runoff from the storm drains and the two rivers has been estimated at about 2.4x10¹¹ L yr⁻¹. This discharge is much smaller than the freshwater discharges from industrial sources (mostly cooling waters from power plants), which amount to about 8x10¹² L yr⁻¹; and the discharges from municipal waste, which are about 1.6x10¹² L yr⁻¹ (Eganhouse and Venkatesan 1993). While surface runoff is highly intermittent and mostly concentrated in the winter months (Dwight *et al.* 2002), municipal wastewater is a continuous source of freshwater. Wastewater is collected by a network of sewers that drain into cen-

Table 1. The coordinates of hydrographic stations and number of observations collected at each station in September 1987-June 1994; total, sea surface temperature (SST), salinity (SAL), dissolved oxygen (O₂), and transmissivity (%T).

Station #	Latitude (°N)	Longitude (°W)	Total	SST	SAL	O ₂	%T
2	33.8178	118.400	351	351	350	327	351
4	33.8244	118.463	348	348	345	323	346
5	33.8481	118.418	348	348	347	323	348
6	33.8519	118.525	352	352	352	329	352
7	33.8519	118.408	347	347	346	324	345
8	33.8686	118.494	346	346	346	324	346
11	33.8822	118.421	351	351	350	327	351
13	33.8931	118.537	345	345	344	320	344
14	33.8944	118.588	353	353	352	330	352
15	33.8967	118.474	343	343	342	319	343
17	33.9050	118.606	350	350	350	327	349
18	33.9075	118.524	351	351	351	327	349
19	33.9114	118.435	346	346	345	322	345
20	33.9117	118.550	346	346	345	325	345
21	33.9147	118.525	351	351	351	328	350
22	33.9200	118.447	349	349	348	325	349
23	33.9214	118.492	347	347	347	323	345
25	33.9281	118.535	350	350	350	326	350
26	33.9283	118.558	351	351	351	327	347
27	33.9378	118.450	347	347	346	324	346
28	33.9411	118.509	350	350	349	327	350
29	33.9422	118.575	355	355	355	331	353
31	33.9528	118.554	353	353	353	330	352
32	33.9606	118.466	354	354	353	328	352
35	33.9719	118.614	354	354	354	331	354
37	33.9861	118.714	348	348	348	324	347
38	33.9897	118.601	351	351	351	328	351
39	33.9911	118.491	349	349	348	325	348
40	33.9964	118.550	360	360	360	336	359
41	33.9972	118.717	355	355	355	332	354
42	33.9978	118.649	347	347	346	324	345
44	34.0069	118.716	353	353	353	330	352
46	34.0200	118.525	350	350	349	326	349
47	34.0242	118.715	349	349	348	325	346
48	34.0306	118.643	350	350	349	326	350
49	34.0317	118.600	349	349	348	326	349

tral treatment plants. Hyperion Treatment Plant is the largest discharging about 5×10^{11} L yr⁻¹ in SMB (Raco-Rands and Steinberger 2001). Its outfall is located 8.3 km offshore at a depth of 57 m (Figure 1).

Variations of hydrographic, chemical, and biological properties in the ocean are a result of several external forces: the exchange of heat across the air-sea interface, the input of mechanical energy into the surface ocean by wind (wind stress), the exchange of freshwater (discharge and air-sea fluxes), the exchange of dissolved gases across the air-sea interface, and the additions of materials by river discharge and atmospheric depositions. The exchange

of heat and freshwater across the air-sea interface leads to changes in surface ocean buoyancy, which drives local mixing and large-scale circulation. The input of momentum by wind stress drives upper ocean currents as well as provides the input of mechanical energy to mix against the vertical stratification. These processes have a pronounced influence on oceanic temperature and salinity. Both wind-driven and buoyancy-driven mixing and circulation, such as that associated with upwelling and entrainment, interact with ocean biological processes. Intense biological production is generated when nutrients, the limiting factor for growth in the study area (Eppley *et al.* 1979, Eppley and Renger 1988), are brought

into the light-illuminated upper ocean. The main biological process, photosynthesis, uses these inorganic nutrients and converts them into organic nutrients, thereby releasing oxygen into the surface ocean. A fraction of the organic matter produced in the upper ocean leaves it as sinking particles or is mixed downward as dissolved organic matter. Most of the organic matter that escapes the surface ocean is remineralized back to inorganic constituents deeper in the water column, using oxygen as the primary oxidation agent. This leads to a reduction of the dissolved oxygen levels below the surface ocean. Oxygen is also exchanged with the atmosphere by gas transfer across the air-sea interface. For conditions typical for SMB, the characteristic time scale for the equilibration of an oxygen anomaly (i.e., a deviation of the dissolved oxygen concentration from saturation) is a few weeks (Broecker and Peng 1974). This timeframe is fast relative to the biogeochemical and physical processes acting in the surface ocean to change oxygen. Therefore, the surface concentration of oxygen is generally relatively close to its saturation value.

While the basic hydrographic and circulation pattern of SMB is well known (Hickey 1992, Hickey *et al.* 2003), the seasonal and interannual variations of these patterns are not well established nor are the mechanisms behind them well understood. Establishing these long-term variations is essential to understanding the high-frequency point observations currently being obtained at the Santa Monica Bay Observatory Mooring, operated by UCLA's Institute of the Environment (Gruber *et al.* in preparation). These data will also be valuable in assessing the impact of future climate change. In this paper, we will focus on hydrographic processes at the ocean surface and utilize the rich spatio-temporal data set collected in Santa Monica Bay between 1987 and 1997 by the L.A. City Environmental Monitoring Division (Dalkey and Shisko 1996). The increasing number of parameters relative to surface properties and their variations that can be monitored by remote sensors from satellites and airplanes (Halpern 2000) provides opportunities for real-time observation and analysis of ecological data. The *in situ* data analyzed and interpreted here will provide a historical background for the analysis of these newly available data.

In this paper, the data set from SMB will be utilized to investigate the imprint of these various processes on the spatio-temporal variations of four parameters: sea surface temperature (SST), salinity

(SAL), dissolved oxygen (O_2), and transmissivity (%T). Our goals are:

- To reveal the general features of the seasonal dynamics of SST, SAL, O_2 , and %T in SMB;
- To study variations of these parameters at sub-seasonal to interannual time scales;
- To analyze the influence of meteorological factors (air temperature, precipitation, wind) on the dynamics of hydrographical parameters in SMB using the statistical method of time-lagged correlation; and
- To explain the observed seasonal anomalies by the influence of both local and remote meteorological and hydrographical factors.

This paper describes the data and statistical methods used for this analysis; analyzes climatological seasonal cycles of the observed data and sub-seasonal variability; and addresses the variability from intraseasonal to interannual time scales.

METHODS

The hydrographic data (SST, SAL, O_2 , and %T) in SMB were collected by the Environmental Monitoring Division of the Los Angeles City Department of Public Works Bureau of Sanitation as part of their program to monitor the water quality of the Hyperion Treatment Plant wastewater discharge. The observations were carried out on a weekly basis from September 1987 through June 1994 and on a monthly basis thereafter until December 1997.

The CTD (conductivity-temperature-depth) profiles were collected over the course of two days throughout SMB at 36 stations from September 1987 to June 1994 and at 32 stations from September 1994 to December 1997 (see Figure 1). All near-shore stations and the northernmost and southernmost offshore stations were sampled on the first day, with the remaining offshore stations sampled on the second day. Profiles of temperature ($^{\circ}C$), salinity (on the practical salinity scale), dissolved oxygen ($\mu\text{mol L}^{-1}$), and transmissivity (%T) were taken using a Sea-Bird Electronics Inc. Model SBE-9 CTD system (Dalkey and Shisko 1996). An analysis of oxygen anomaly, defined as the deviation of the measured oxygen concentration from the oxygen saturation, was conducted in lieu of an analysis of dissolved oxygen concentration. This approach was selected based on the fast exchange of oxygen across the air-sea interface, which results in surface ocean oxygen levels close to saturation. The oxygen solubility function of

Garcia and Gordon (1992) was used to estimate the oxygen anomaly on the basis of the CTD-measured dissolved oxygen concentrations, temperature, and salinity. Oxygen anomalies (hereafter ΔO_2) are expressed in $\mu\text{mol L}^{-1}$.

Station coordinates and the number of observations collected at each station are given in Tables 1 and 2. In most surveys, all stations were sampled at least once. Some stations were sampled twice, which is why the total number of observations exceeds the total number of surveys in a few cases (410). Temperature, salinity, and transmissivity were measured at almost all stations; oxygen at >90% of stations.

In order to assess the spatial structure of the variations and remove the effect of the change in the sampling grid, the four parameters (SST, SAL, ΔO_2 , and %T) were interpolated for each survey onto a regular grid of 0.01° resolution within the latitude range $33.76\text{--}34.06^\circ\text{N}$ ($33^\circ45.6'\text{--}34^\circ03.6'\text{N}$) and longitude range $118.74\text{--}118.38^\circ\text{W}$ ($118^\circ44.4'\text{--}118^\circ22.8'\text{W}$). The interpolation was carried out using the kriging method (Isaaks and Srivastava 1989, Oliver and Webster 1990). Grid nodes that are located more than 5 km from the nearest sampling station were excluded from the analysis.

The four parameters exhibit distinct seasonal variations, which can be approximated by a harmonic function with a 12-month period. In order to construct a mean seasonal climatology, we fitted a harmonic function of the type

$$y = m - k * \cos((t - \varphi) * 2\pi / 365), \quad (1)$$

to all four parameters at each node with observations. In (1) y is SST, SAL, ΔO_2 , or %T; t is Julian day; m is the mean value of the parameter; k represents the amplitude of the seasonal cycle; and $-\varphi$ is the phase illustrating the time when the seasonal minimum occurs.

Next, seasonal anomalies were computed by removing the climatological mean seasonal cycle from the observed time series, both integrated over the entire SMB and at each grid node. From those seasonal anomalies, interannual anomalies were created by filtering the seasonal anomalies with a 100-d running mean filter. The seasonal anomalies were analyzed further using the method of empirical orthogonal functions (EOF). The EOF method decomposes the spatio-temporal variability into a set

of orthogonal functions (spatial maps) and the corresponding principal components (time series). Each of these orthogonal functions is ranked by their temporal variance. Ideally, the leading order orthogonal functions explain a substantial fraction of the total variance, so that the sum is a close reconstruction of the initial signal. The methodology is described in Priesendorfer (1988).

Air temperature (hereafter T_{air}) was measured at the meteorological station of the Los Angeles International Airport (LAX). This station is located 3 miles (5 km) to the east of the SMB shore (Figure 1). Marine air covers the coastal plain most of the year, and thus the air temperature at LAX does not differ greatly from the air temperature over SMB. The LAX T_{air} data was compared with the air temperatures obtained in the central part of SMB by the UCLA Institute of the Environment Bay Observatory Mooring in June 2001–April 2003 (Gruber *et al.* in preparation); both time series were highly correlated ($r=0.9185$; $p<0.001$); the difference averaged 0.76°C . The mean seasonal cycle was estimated by approximating the observations using Equation 1, and seasonal anomalies were obtained by subtracting this mean seasonal cycle.

Surface freshwater discharge to SMB originates from the atmospheric precipitation over the watershed area. An important aspect of the climate of the Los Angeles metropolitan area is the pronounced difference in weather conditions including precipitation over fairly short distances, which is closely related to the distance from, and elevation above, the Pacific Ocean. Precipitation generally increases with distance from the ocean, from a yearly total of around 300 mm in the coastal sections to the south of the city of Los Angeles to over 500 mm in the foothill areas. To obtain more reliable values of freshwater discharge from surface runoff, the total rainfall over the watershed was estimated from the meteorological observations at 5 stations, when the complete record of observations during 1987–1997 (4,018 d) was available (Table 3, Figure 1). The daily precipitation (hereafter Pr) at 5 stations was averaged and smoothed using a 7-d running average to enable time-lagged correlation analysis between daily precipitation and weekly oceanographic observations.

To determine representative wind stress variations over a relatively large region, wind stresses determined from atmospheric pressure fields were used rather than from the relatively sparse *in situ* wind speed measurements. More specifically, offshore and

Table 2. The coordinates of hydrographic stations and number of observations collected at each station in September 1994–December 1997; total, sea surface temperature (SST), salinity (SAL), dissolved oxygen (O₂), and transmissivity (%T).

Station #	Latitude (°N)	Longitude (°W)	Total	SST	SAL	O ₂	%T
1	33.7914	118.451	37	37	37	36	37
3	33.8231	118.517	38	38	38	37	38
4	33.8244	118.463	39	39	39	38	37
5	33.8481	118.418	41	41	41	40	41
6	33.8519	118.525	43	43	43	42	41
8	33.8686	118.494	49	49	49	48	49
9	33.8792	118.536	57	57	57	55	57
10	33.8792	118.457	41	41	41	40	40
12	33.8867	118.506	58	58	58	56	58
15	33.8967	118.474	56	56	56	54	55
16	33.9000	118.453	40	40	40	39	40
18	33.9075	118.524	62	62	62	60	62
20	33.9117	118.550	59	59	59	58	59
21	33.9147	118.525	64	64	64	62	63
22	33.9200	118.447	41	41	41	40	40
23	33.9214	118.492	59	59	59	57	57
24	33.9253	118.467	40	40	40	39	40
25	33.9281	118.535	63	63	63	61	63
26	33.9283	118.558	58	58	58	56	57
28	33.9411	118.509	56	56	56	55	54
29	33.9422	118.575	56	56	56	54	56
30	33.9519	118.485	39	39	39	38	39
31	33.9528	118.554	63	63	63	61	62
33	33.9664	118.526	42	42	42	41	42
34	33.9714	118.565	45	45	45	44	45
35	33.9719	118.614	38	38	38	37	38
36	33.9764	118.505	39	39	38	37	38
38	33.9897	118.601	39	39	39	38	39
41	33.9972	118.717	40	40	40	39	40
42	33.9978	118.649	41	41	41	40	41
43	34.0058	118.597	39	39	39	38	39
45	34.0175	118.716	40	40	40	39	39

alongshore components of the “Bakun upwelling index” (Bakun 1973) were used for the location 33°N, 119°W (obtained from the Pacific Fisheries Environmental Laboratory (PFEL) <http://www.pfeg.noaa.gov/>). Though expressed in units of water transport ($\text{m}^3 \text{s}^{-1}$ per 100 m of the coastline), the upwelling index is directly proportional to wind stress. The offshore upwelling index is a measure of the equatorward alongshore wind stress, and the alongshore upwelling index is a measure of the wind stress directed onshore. The coastal angle used by PFEL at 33°N is 129°; i.e., the equatorward wind is northwesterly and onshore wind is southwesterly. Based on the limitation that wind stresses are only indirectly determined, the alongshore wind stress toward the equator is referred to as WS_{eq} and the onshore component as WS_{on} . The seasonal variations of WS_{eq} and WS_{on} were approximated by

Equation 1 (Figures 2g, h) to obtain seasonal anomalies.

In order to investigate the influence of large-scale/low-frequency forcing on the observed variability in SMB more explicitly, lag correlations were computed of low pass filtered time-series with an index of the ENSO phenomenon. In particular, the seasonal anomaly time series of each parameter was smoothed with a 100-d running mean filter in order to obtain an interannual anomaly time series. We used the NINO3 index as our index for ENSO, which was determined by averaging the SST anomalies over the eastern tropical Pacific (5°S–5°N; 150°W–90°W). The values were obtained from the International Research Institute of Climate Prediction (<http://iri.ldeo.columbia.edu/>).

Table 3. Location of meteorological stations where atmospheric precipitation was measured.

Station	Latitude	Longitude	Elevation above sea level (m)
Long Beach Daugherty Field	33°49'N	118°09'W	9.4
Los Angeles International Airport (LAX)	33°56'N	118°23'W	29.6
Los Angeles Downtown	34°03'N	118°14'W	70.1
Pasadena	34°09'N	118°09'W	263.3
Torrance Municipal Airport	33°48'N	118°20'W	33.5

RESULTS

Seasonal climatology: Annual mean distribution and variability

The spatial distributions of the annual mean SST, SAL, ΔO_2 , and %T in SMB are illustrated in Figure 3. Annual mean SST varies between 16.6°C and 17.5°C with the highest values observed in the southern inshore part of SMB and the lowest SST found in the northern part, a few kilometers offshore (see also Table 4 for mean values). Annual mean salinity is relatively uniform across the entire Bay, with values close to 33.40, except for a zone of low salinity along the coast with the lowest values found near the mouth of Ballona Creek. The annual mean oxygen anomaly shows a substantial supersaturation across the entire SMB with values between +16 to +28 $\mu\text{mol L}^{-1}$ (equivalent to a relative supersaturation of 6 to 11%). The spatial distribution of the annual mean ΔO_2 reveals generally higher values in the nearshore region, except for the very inshore region in the southern part of the Bay, and lower supersaturations in the deep central part of SMB. The annual mean transmissivity (%T) in SMB is medium to high, with values between 66% in the inshore region, tapering off to values above 85% offshore.

Figure 4 illustrates the spatial distribution of the standard deviation (SD) around the annual mean of SST, SAL, ΔO_2 , and %T in SMB. Maximum variability of SST, SAL, and %T occurs in a narrow zone near the shore. In the case of ΔO_2 , the zone of high variability is much wider and more irregular.

Seasonal climatology: Seasonal variations

Figures 5 and 6 illustrate the spatial distribution of the amplitude and phasing of the mean seasonal cycle (coefficients k and φ in Equation 1) of SST, SAL, ΔO_2 , and %T over the SMB area. In general, the seasonal amplitudes of all parameters are of similar magnitude as the standard deviation (Figure 4), suggesting that most of the total variability is caused by the sea-

sonal cycle. Although the seasonal amplitude is relatively small in comparison to the mean value and to amplitudes observed in other oceanic regions, the spatial distribution of the amplitude shows a distinct spatial distribution. The amplitudes of SST, SAL, and %T (Figure 5) are highest in the nearshore zones and tend to decrease offshore. In the cases of SAL and %T, these zones are located near Marina Del Rey, indicating that Ballona Creek acts as a main source of seasonal variations for both salinity and turbidity. The seasonal amplitude of the oxygen anomaly is of about equal magnitude as the mean, and with a pattern that resembles that of the mean. The Ballona Creek region differs in that regard in that the seasonal amplitude of ΔO_2 is strongly suppressed relative to the rest of the Bay.

The seasonal phasing of the different parameters is quite different (see Figure 2 and Table 4), with SST and SAL having their seasonal minima in mid-February (Julian Day 49) and late January (Julian Day 24), respectively, while the seasonal minimum of ΔO_2 occurs in late December (Julian Day 362) and that of %T at the end of April (Julian Day 118). The occurrence of the seasonal minima of SST, SAL, and ΔO_2 varies across SMB by more than two weeks (Figure 6). The seasonal minimum (and maximum) of SST and %T generally occur earlier in the inshore compared to offshore.

The following exceptions apply for SAL: the observation of a conspicuous early minimum in the seasonal cycle of SAL in the central part of SMB, just over the Hyperion Treatment Plant outfall; and the “latest” seasonal minimum of SAL, observed inshore near Marina Del Rey and to the east of Malibu Point. For ΔO_2 , seasonal extremes are

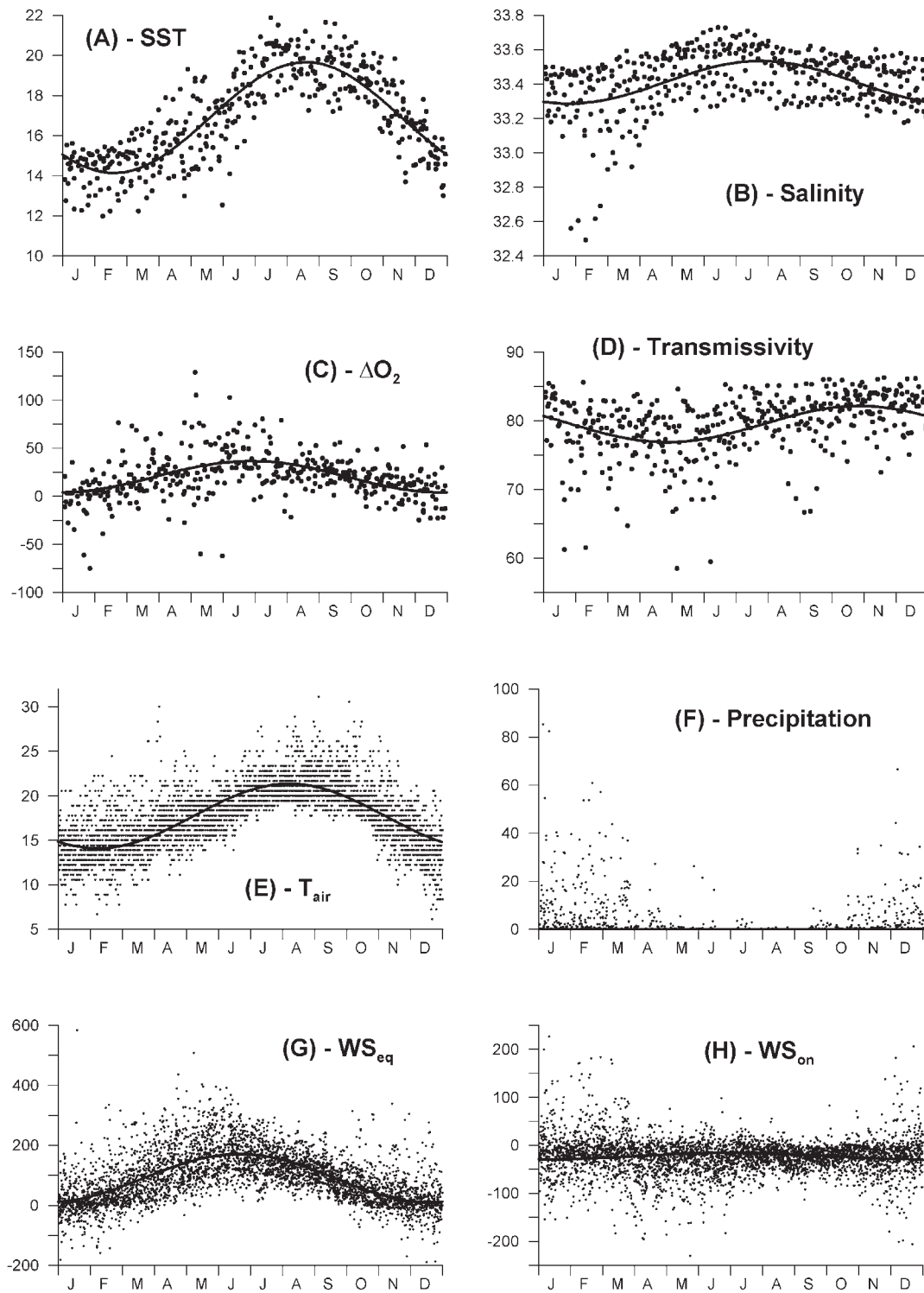


Figure 2. Seasonal variations of (a) sea surface temperature ($^{\circ}\text{C}$), (b) salinity, (c) oxygen anomalies ($\mu\text{mol/L}$), and (d) transmissivity ($\%T$) in Santa Monica Bay. (e) Air temperature at Los Angeles International Airport (LAX) ($^{\circ}\text{C}$), (f) precipitation averaged over 5 stations in the north-western portion of the Los Angeles Basin (mm/day), (g) equatorward and (h) onshore wind stress ($\text{m}^3 \text{s}^{-1}$ per 100 m of the coastline). The lines show the seasonal variations approximated by Equation 1 in the main text.

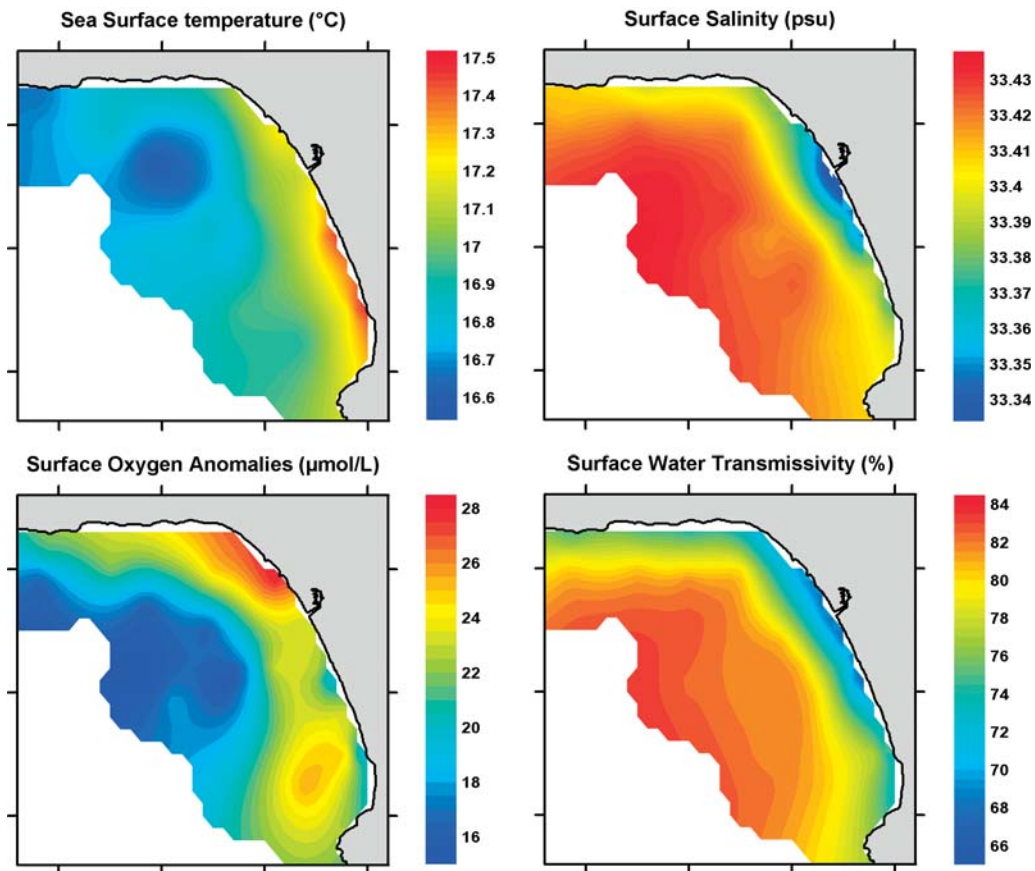


Figure 3. Annual mean spatial distribution of SST (°C), SAL, ΔO_2 ($\mu\text{mol/L}$), and %T (%) in SMB averaged over the entire period of observations (1987-1997).

observed first in the southern part of SMB. In Marina Del Rey and the northwestern part of the basin, the seasonal minimum occurs three to four weeks later. The largest variations in phasing are found for %T, which varies by more than two months over the Bay. The seasonal minimum of T_{air} (Figure 2e) is observed in early February (Julian Day 38) and its maximum in early August (Julian Day 220). The seasonality of Pr is strong, with a maximum in winter and essentially zero Pr in summer. The seasonal maximum of WS_{eq} occurs about June 21 (Julian Day 172) and the minimum about December 20 (Julian Day 354). The seasonal minimum of WS_{on} is observed at the beginning of January (Julian Day 2) and the maximum at the beginning of July (Julian Day 185). However, the latter cycle is not pronounced.

Sub-seasonal variability: Time-series of the seasonal anomalies

The temporal variations of the seasonal anomalies of SST, SAL, ΔO_2 , and %T averaged over the SMB area are shown in Figure 7. For SST, ΔO_2 , and %T, sub-seasonal variability tends to dominate over longer term variations. In contrast, variations of SAL over the entire SMB are more persistent; leading to the domination of long-term variability over sub-seasonal variations.

Table 5 indicates correlations between the seasonal anomalies of SMB mean SST, SAL, ΔO_2 , %T, and various meteorological forcings. Significant correlations are observed between SST, SAL, and %T; high SAL is accompanied by low SST and high %T. As for the correlations with meteorological forcings, the highest correlation (+0.40) is found between air temperature and SST. A negative correlation exists between SAL and Pr; a second factor forcing salinity variations is wind.

Table 4. The coefficients of Equation 1 for sea surface temperature (SST), salinity (SAL), oxygen anomaly (ΔO_2), transmissivity (%T), air temperature (T_{air}), equatorward wind stress (WS_{eq}), and onshore wind stress (WS_{on}).

	m	k	φ (Julian Day)
Sea surface temperature ($^{\circ}C$)	16.90	2.761	48.78
Salinity (psu)	33.41	0.124	24.03
Oxygen anomaly ($\mu mol/L$)	20.4	16.36	361.81
Transmissivity (%)	79.52	2.634	117.85
Air temperature ($^{\circ}C$)	17.72	3.624	37.69
WS_{eq} ($m^3 s^{-1}$ per 100 m of the coastline)	90.64	80.376	354.76
WS_{on} ($m^3 s^{-1}$ per 100 m of the coastline)	-22.19	6.786	2.49

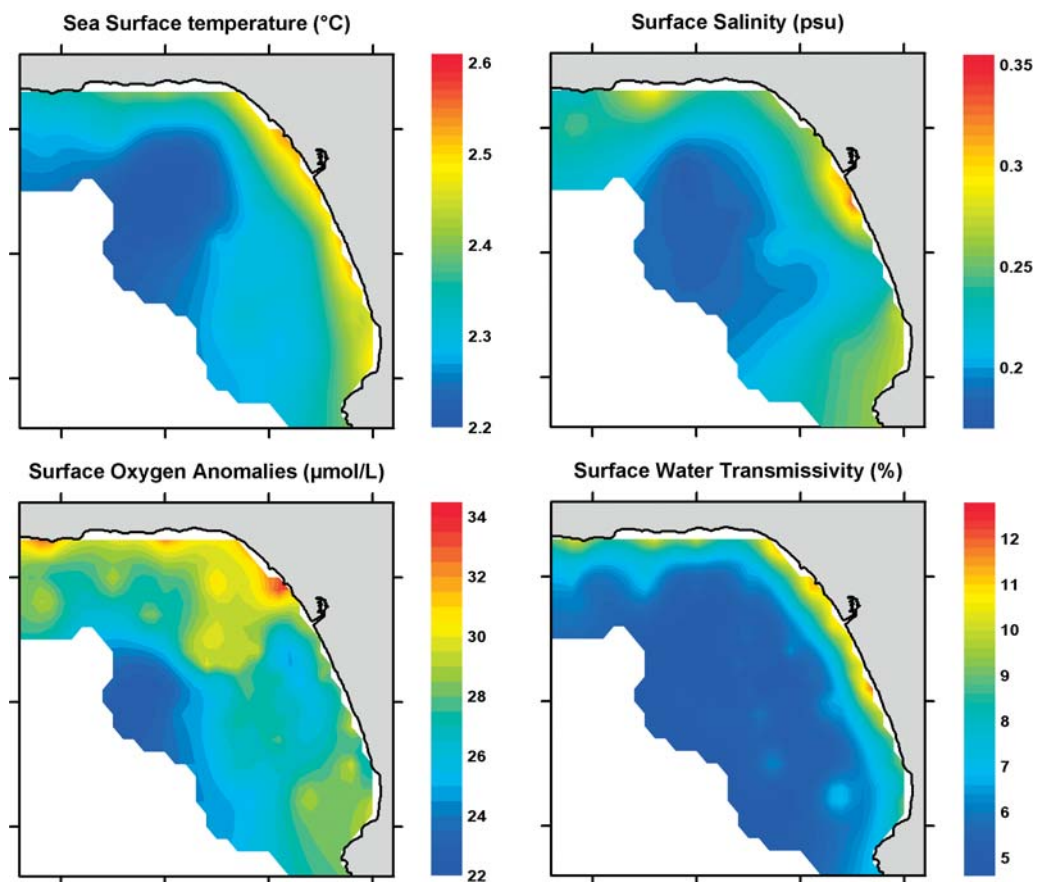


Figure 4. Spatial distribution of the total variability (standard deviation, SD) of SST ($^{\circ}C$), SAL, ΔO_2 ($\mu mol/L$), and %T (%) in SMB over the entire period of observations (1987-1997).

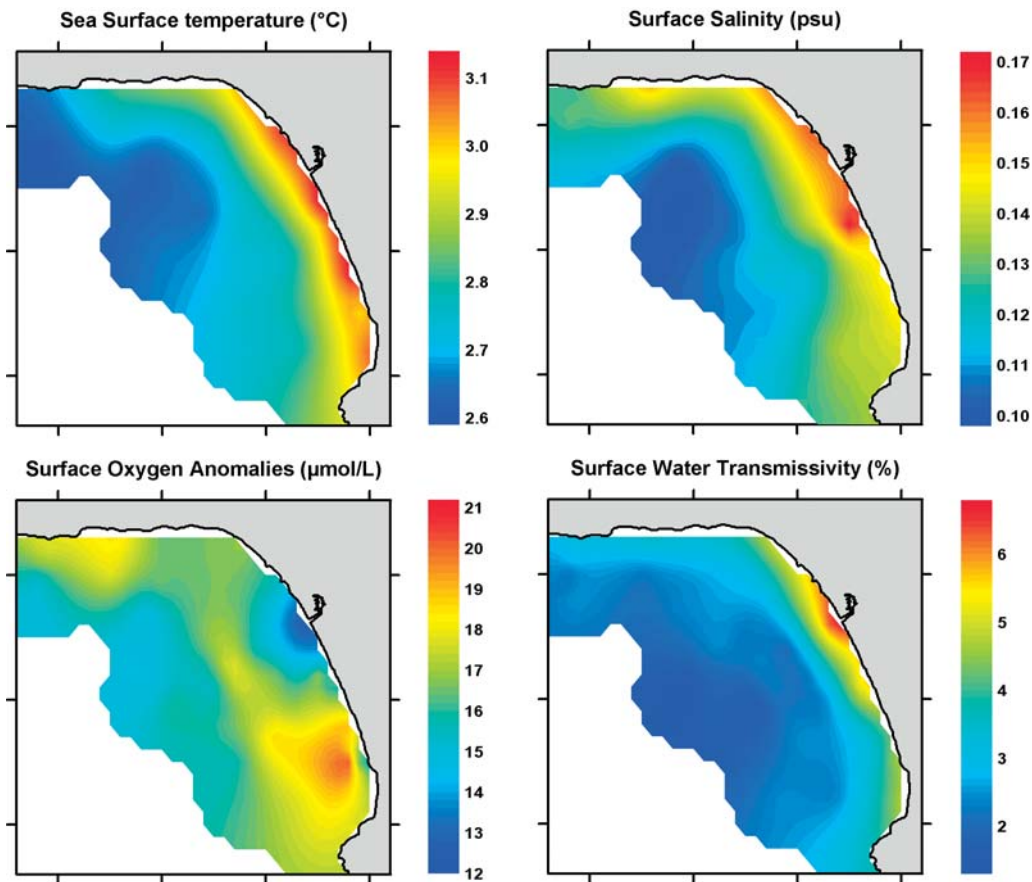


Figure 5. Spatial distribution of the amplitude of seasonal variations of SST (°C), SAL (psu), ΔO_2 ($\mu\text{mol/L}$), and %T (%) in SMB estimated from the entire period of observations (1987-1997). Note that the amplitude is defined as the coefficient k of Equation 1; the seasonal difference between the minimum and maximum is twice the amplitude.

Sub-seasonal variability: EOF analysis of the seasonal anomalies

Table 6 illustrates the contribution of the 10 leading EOF modes to the total non-seasonal variability of SST, SAL, ΔO_2 , and %T over the SMB area. For each parameter, the three leading EOF modes were selected for analysis. They contribute 58.0%, 51.3%, 49.8%, and 50.2% to total variability of SST, SAL, ΔO_2 , and %T, respectively. The remaining modes contribute little to the total non-seasonal variability and reveal neither clear pattern nor correlations with meteorological factors.

The patterns of the first EOF modes of all four parameters are remarkably similar (Figure 8), revealing a nearshore to offshore gradient with higher SST (Figure 8a), SAL (Figure 8c), ΔO_2 (Figure 8g), and %T (Figure 8e) located in a narrow inshore area.

This mode is referred to as “the onshore/offshore” mode. The patterns of the second EOF modes show a gradient between the northwestern and southeastern parts of SMB. In this mode, the northwestern area is occupied by low values of SST (Figure 8b), SAL (Figure 8d), and %T (Figure 8h); and high values of ΔO_2 (Figure 8f) anomalies. This mode is called “the north/south” mode. The third EOF modes illustrate the differences between the central part of SMB and its northwestern and southeastern zones. The maxima of the third EOF modes for SAL and %T are located in Marina Del Rey; the maximum of SST and the minimum of ΔO_2 are located a few kilometers offshore. Evidently, the discharge from Ballona Creek seems to be a main factor regulating the spatio-temporal variability revealed in the third EOF modes. Therefore, this mode is referred to as “the discharge” mode.

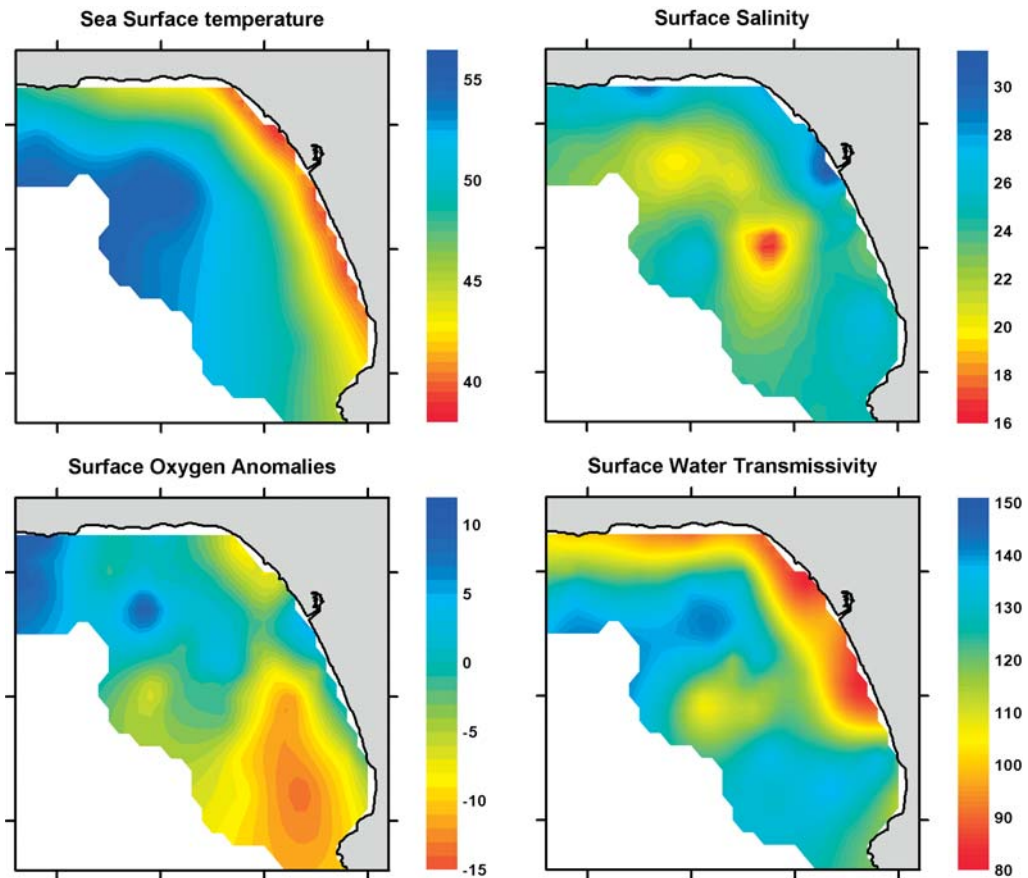


Figure 6. Spatial distribution of the seasonal phase (coefficient φ of Equation 1, Julian Day) of SST, SAL, ΔO_2 , and %T in SMB estimated from the entire period of observations (1987-1997).

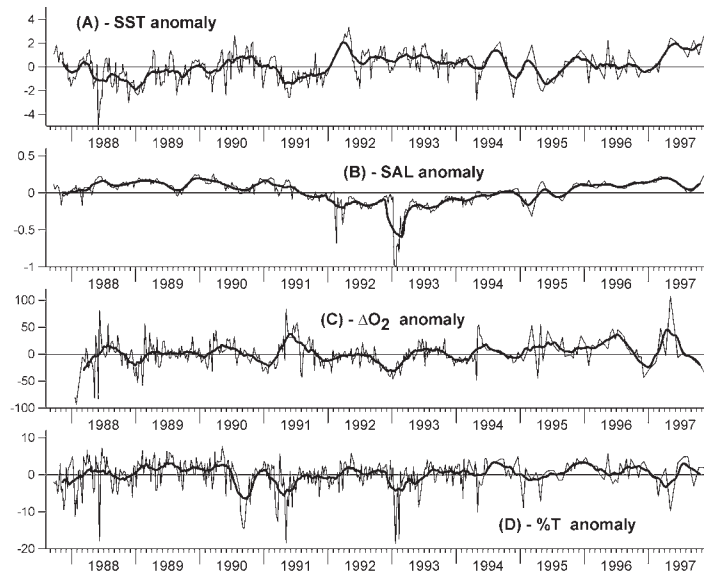


Figure 7. Temporal variations of (a) sea surface temperature, (b) salinity, (c) oxygen anomaly, and (d) transmissivity seasonal anomalies averaged over SMB. Thick solid lines indicate the results of smoothing using 100-d linear filter.

Table 5. Coefficients of linear correlation between the external forcing WS_{eq} , WS_{on} , T_{air} , Pr and NINO3 SAL, ΔO_2 , and %T averaged over SMB. Only significant ($p < 0.05$) coefficients are given. The coefficients of high significance ($p < 0.001$) are marked with bold.

	WS_{eq}	WS_{on}	T_{air}	Pr	SST	SAL	ΔO_2
	1.00	X	X	X	X	X	X
WS_{eq}	-0.226	1.00	X	X	X	X	X
WS_{on}	-0.376	-0.168	1.00	X	X	X	X
T_{air}	-	+0.269	-0.188	1.00	X	X	X
Pr	-0.103	+0.121	+0.402	-	1.00	X	X
SST	+0.148	-0.213	-	-0.263	-0.265	1.00	X
SAL	-	-	+0.101	-0.209	-	+0.112	1.00
ΔO_2	-	-	-	-0.191	+0.173	+0.291	-
%T	-	-	-	-	-	-	0.116

Figure 9 shows the temporal variations of the principal components of the two leading (“inshore/offshore” and “north/south”) EOF modes for SST, SAL, ΔO_2 , and %T from 1987 to 1997. Temporal variations of the equatorward and onshore wind stress, air temperature, atmospheric precipitation, and NINO3 index are depicted in Figure 10.

Sub-seasonal variability: Correlations between the EOF modes

Correlations were found between the principal components of the first, second, and third EOF modes for all four parameters (SST, SAL, ΔO_2 , and %T). For most correlations, the maxima are at zero time lag.

Significant correlations are shown in Table 7. Figure 11 shows the time lag correlation for the discharge modes of SAL and ΔO_2 , which represents the only parameter pair that had significant correlations at time lags different from zero.

The inshore/offshore EOF modes of SST, SAL, and %T are positively correlated with each other. The inshore/offshore mode of ΔO_2 is not significantly correlated with SST and SAL, but is negatively correlated with %T. This means that the anomalously

Table 6. The percentage of variation of sea surface temperature (SST), salinity (SAL), oxygen anomalies (ΔO_2), and transmissivity (%T), explained by 10 leading modes of empirical orthogonal functions (EOF) analysis (in parenthesis cumulative percent).

EOF mode	SST	SAL	ΔO_2	%T
1	23.70 (23.70)	29.79 (29.79)	21.43 (21.43)	25.20 (25.20)
2	21.93 (45.63)	13.09 (42.88)	17.74 (39.17)	15.54 (40.74)
3	12.34 (57.97)	8.42 (51.31)	10.29 (49.46)	9.50 (50.24)
4	8.90 (66.86)	6.53 (57.84)	7.40 (56.86)	6.57 (56.82)
5	6.69 (73.56)	5.80 (63.64)	5.53 (62.38)	5.48 (62.30)
6	4.90 (78.45)	4.59 (68.23)	4.86 (67.24)	4.67 (66.96)
7	3.11 (81.56)	4.07 (72.30)	4.04 (71.28)	3.66 (70.62)
8	2.54 (84.10)	2.93 (75.23)	3.34 (74.62)	3.36 (73.99)
9	1.97 (86.07)	2.55 (77.78)	3.16 (77.77)	2.88 (76.87)
10	1.78 (87.85)	2.28 (80.07)	2.86 (80.64)	2.56 (79.42)

high SSTs that are associated with this onshore-offshore mode near the coast tend to coincide with high salinities and transmissivities, and low oxygen anomalies. However, most of these correlations are relatively weak. The exceptions are the correlations between SAL and %T and between ΔO_2 and %T.

The correlations of the north/south EOF mode are also positive (Table 7). The correlations reveal that the anomalously low SSTs found in the northwestern part of SMB during the positive phases of this north-

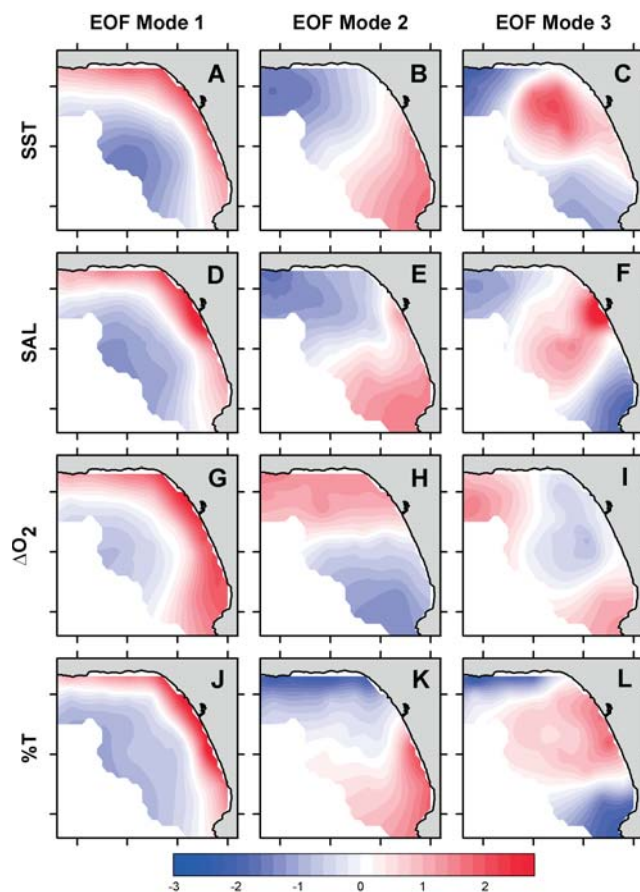


Figure 8. Spatial maps of the three leading EOF modes of subseasonal variability in SMB. The three columns show the first (inshore/offshore mode), the second (north/south mode), and the third EOF (discharge mode) for the various quantities. (a)-(c) three leading EOFs for the seasonal anomalies of sea surface temperature (SST); (d)-(f), as (a) but for salinity (SAL); (g)-(i), as (a) but for oxygen anomaly (ΔO_2); (j)-(l), as (a) but for transmissivity (%T).

south mode are generally accompanied by low salinities, high oxygen anomalies, and low water transparencies.

The correlations for the “discharge” mode are small; variations in SAL are weakly positively correlated with SST, ΔO_2 and %T variations. These correlations (Table 7) reveal that an increase of salinity in the zone of influence of the Ballona Creek discharge is correlated with a decrease of ΔO_2 and an increase of water transparency. The maximum of correlation between SAL and ΔO_2 has a time lag different from zero (Figure 11); ΔO_2 was trailing SAL within 10 to 20 d.

Sub-seasonal variability: Correlations between the EOF modes and the meteorological factors

In order to investigate the causes underlying these modes, such as local meteorological forcing, ocean internal dynamics, or remote influences, we studied the time-lagged correlations between the EOF modes and several meteorological factors.

The inshore/offshore EOF mode of SAL is negatively correlated with Pr (Figure 12a) and WS_{on} (Figure 12b), with Pr leading the variations of salinity by 0 to 20 d and WS_{on} by 0 to 30 d. The inshore/offshore EOF mode of SST is positively correlated with Pr (Figure 12d); SST variations lead Pr variations from 0 to >30 days. The inshore/offshore EOF mode of %T is negatively correlated with Pr (Figure 12e). This weak correlation is expected given the strong positive correlation between the inshore/offshore EOF modes of salinity and %T.

The north/south EOF mode of SST is negatively correlated with Pr, within a wide range of time lags (Figure 12g). The north/south EOF mode of SAL is positively correlated with Pr (Figure 12h), the latter leading SAL by 0 to 15 d.

Intraseasonal to interannual variability

Visual inspection of the time-series of the various properties and their EOF modes (Figures 7 and 9) shows a substantial amount of low frequency variability. The possible roles of various processes in forcing this part of the variability spectrum are addressed in the following paragraphs.

Table 8 shows the zero-time lag correlation coefficients of the interannual anomalies with various atmospheric and oceanic forcings. The first part of the table refers to the mean anomalies over the entire Bay, computed by averaging the properties over the investigated region for any given survey. The second part of the table refers to the interannual anomalies of the three leading EOF modes. A comparison of these interannual anomaly correlations (Table 8) with those obtained for the sub-seasonal anomalies (Tables 5 and 7), shows generally larger correlations. This needs to be viewed cautiously, since with 10 years of data, there are many fewer degrees of freedom for interannual variability correlations. Fewer degrees of freedom require much larger values of the correlation coefficient in order to be significant. Keeping this caveat in mind, a number of high correlations are particularly noteworthy. On timescales longer than a few months, SST is strongly correlated with wind stress, air temperature, and the NINO3

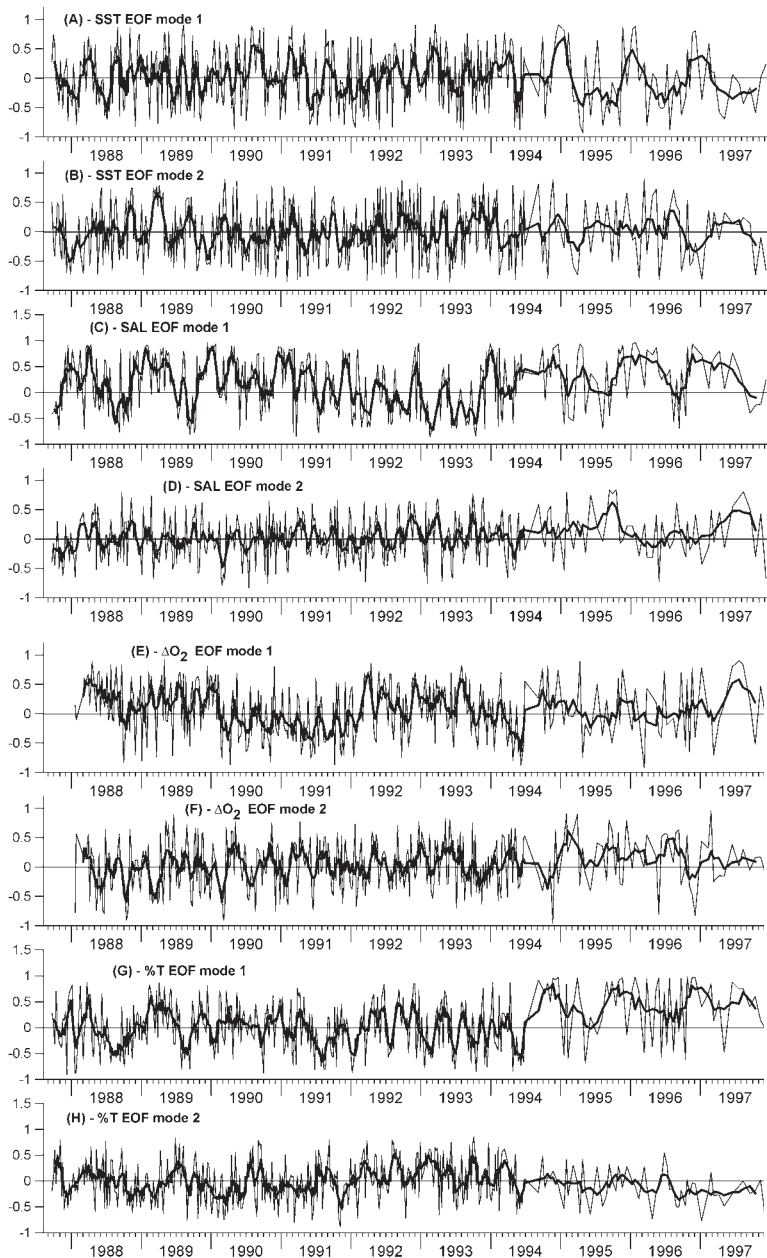


Figure 9. Time series of the principal components of the two leading EOF modes for (a)-(b) sea surface temperature; (c)-(d) salinity; (e)-(f) oxygen anomaly; and (g)-(h) surface ocean transmissivity. Thick solid lines indicate the results of smoothing using 100-day linear filter.

index. By contrast, the correlation with precipitation is very small. Salinity shows high correlations with wind stress and precipitation, but is only weakly related to air temperature. The signs of the correlations between SST, SAL, and the two wind stresses are of interest. Stronger than normal equatorward wind stress leads to lower SSTs and higher SAL and vice versa; while stronger than normal onshore wind

stress leads to warmer SSTs and lower SAL values. The oxygen anomaly shows only a noteworthy correlation with precipitation, while transmissivity does not exhibit any strong correlations. The correlations between the external forcings and the EOF modes are much higher for the interannual variability frequency band (Table 8) than they are for the unfiltered data, i.e. subseasonal frequency band (Table 7).

The most pronounced correlations are observed between the third (“discharge”) EOF mode of SST and all external forcings excluding Pr; the highest correlation (-0.63) is with the NINO3 index.

Atmospheric precipitation influences the “inshore/offshore” SST EOF mode (+0.44), indicating freshwater discharge is a substantial source of the temperature gradient. The onshore wind stress mostly influences the “north/south” ΔO_2 EOF mode (+0.41) and the equatorward wind stress is positively correlated with the “north/south” %T EOF mode (+0.36).

DISCUSSION

Seasonal Climatology: Annual mean distribution

The observed distribution of the annual mean SST in SMB is likely due to a combination of an offshore/onshore gradient in SST, caused by stronger sheltering in the near-shore regions and possible warming from the beach zone, and a general north-south gradient in SST. The latter is likely reinforced by the interaction of the southward flowing branch of the cold California Current, which penetrates into SMB from the northwest and the northward flowing Southern California Countercurrent, which penetrates into SMB from the south (Hickey 1992, 1993, Hickey *et al.* 2003).

In contrast to the annual mean SST distribution, the spatial distribution of the annual mean salinity is dominated by the freshwater discharge from Ballona Creek. This conclusion is corroborated by the pattern of SAL variability, which shows highest variability near Marina Del Rey.

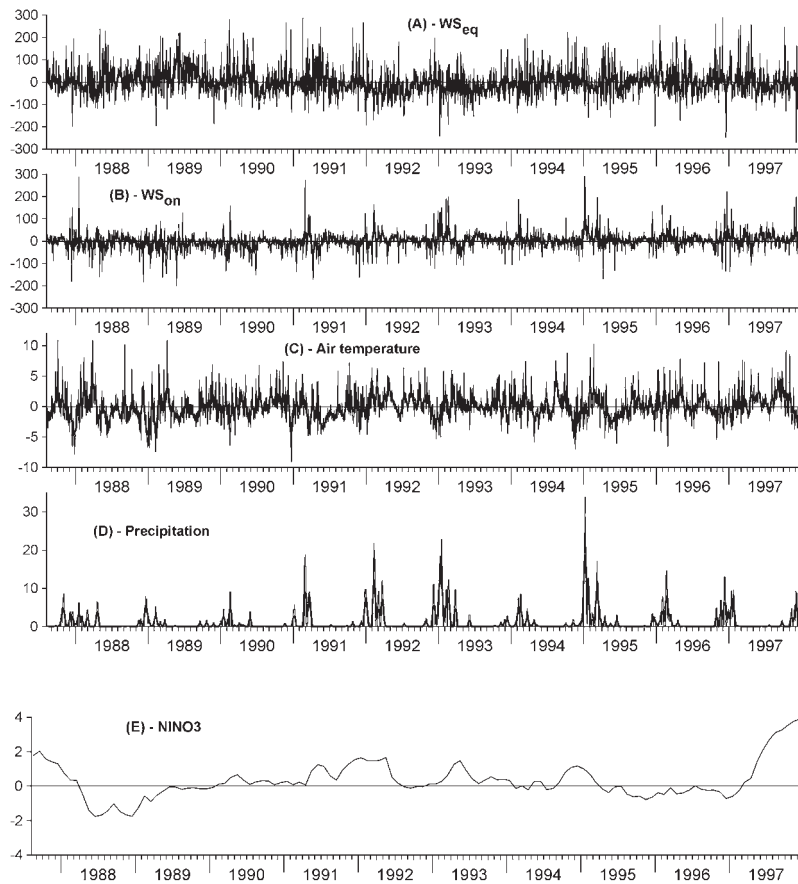


Figure 10. Temporal variations of (a) equatorward and (b) onshore wind stress anomalies ($\text{m}^3 \text{s}^{-1}$ per 100 m of the coastline); (c) air temperature seasonal anomalies ($^{\circ}\text{C}$); (d) atmospheric precipitation (mm/day); and (e) NINO3 index. See text for data sources. Thick solid lines indicate the results of smoothing using 100-day linear filter.

The first remarkable observation about the ΔO_2 distribution within SMB is its general supersaturation. The only two processes that can lead to such a supersaturation are (1) net heating of the surface ocean layer and (2) generation of oxygen by photosynthesis. We suspect that biological processes are primarily responsible for maintaining the high ΔO_2 values in winter and early spring when the surface ocean is generally cooling, and that net heating maintains the supersaturation in summer against the continuous loss of oxygen from the surface ocean into the atmosphere by air-sea exchange.

The general trend toward higher oxygen annual mean ΔO_2 in the nearshore zones is likely due to enhanced biological productivity, probably driven by higher nutrient input because of enhanced vertical mixing, closeness of the bottom sediments, and

nutrient inputs from the wastewater discharge. We cannot explain the anomalously low ΔO_2 values in the southern nearshore zone of SMB. One possible reason is enhanced oxygen demand from the remineralization of organic matter that is being brought into the marine environment from external sources.

Seasonal climatology: Seasonal variations

The spatial distributions of the seasonal amplitude of SST, SAL, and %T (Figure 5) are similar to the spatial distribution of their total variability (Figure 4), but the inshore zones of high seasonal variability occupy larger areas compared to total variability. For SAL and %T, these zones are located near Marina Del Rey, indicating that Ballona Creek is a main source of seasonal variations of both salinity and transparency in the surface layer.

For ΔO_2 , the spatial patterns of seasonal and non-seasonal variability are somewhat different, in line with the observation that the seasonal variations represent a smaller fraction of the total variability, compared to the other parameters. The magnitude of the seasonal amplitude increases generally toward the shores, with the highest seasonal amplitude of ΔO_2 observed in the southeastern part of SMB, over

Redondo Canyon. A remarkable deviation from this general trend is the very small seasonal amplitude observed near Marina Del Rey, in the zone of influence of the Ballona Creek discharge. The tendency for a higher seasonal amplitude in the nearshore zones is in line with the general increase in the annual mean ΔO_2 toward the shores, which we interpreted as a result of generally higher productivity levels fueled by higher level of mixing in the nearshore environments. We interpret the low seasonal amplitude of the regions around the mouth of Ballona Creek to be caused by the input of oxygen rich freshwaters into SMB during winter time, when the rest of SMB experiences low levels of ΔO_2 as a result of general cooling and the entrainment of low ΔO_2 levels from the thermocline. The reduction of the sea-

Table 7. Coefficients of linear correlation between the three leading EOF modes of SST (SST-1, SST-2, SST-3), SAL (SAL-1, SAL-2, SAL-3), ΔO_2 (ΔO_{2-1} , ΔO_{2-2} , ΔO_{2-3}), %T (%T-1, %T-2, %T-3) and meteorological factors WS_{eq} , WS_{on} , T_{air} and Pr. Only significant ($p < 0.05$) coefficients are given. The coefficients of high significance ($p < 0.001$) are marked with bold.

	SST-1	SST-2	SST-3	SAL-1	SAL-2	SAL-3	ΔO_{2-1}	ΔO_{2-2}	ΔO_{2-3}	%T-1	%T-2	%T-3	WS_{eq}	WS_{on}	T_{air}
SST-1	1.00	X	X	X	X	X	X	X	X	X	X	X	X	X	X
SST-2	-	1.00	X	X	X	X	X	X	X	X	X	X	X	X	X
SST-3	-	-	1.00	X	X	X	X	X	X	X	X	X	X	X	X
SAL-1	+0.142	-	-	1.00	X	X	X	X	X	X	X	X	X	X	X
SAL-2	-	+0.222	-0.112	-	1.00	X	X	X	X	X	X	X	X	X	X
SAL-3	-0.190	-	+0.150	-	-	1.00	X	X	X	X	X	X	X	X	X
ΔO_{2-1}	-	-	-0.142	-	-0.161	-	1.00	X	X	X	X	X	X	X	X
ΔO_{2-2}	-	-	-	-	+0.206	-	-	1.00	X	X	X	X	X	X	X
ΔO_{2-3}	-	-	-	-	-	+0.150	-	-	1.00	X	X	X	X	X	X
%T-1	-	-	-	+0.344	+0.170	-	-0.269	-	-	1.00	X	X	X	X	X
%T-2	+0.132	-	-	-0.177	+0.186	-	-0.132	+0.188	-	-	1.00	X	X	X	X
%T-3	-	-	-0.103	-0.110	-	+0.140	-	-	-	-	-	1.00	X	X	X
WS_{eq}	-	+0.130	-	-	-	-	-	+0.112	-0.122	-0.139	-	-	1.00	X	X
WS_{on}	-	-	-0.115	-0.191	-	-	-	-	-	+0.276	-	-	-0.226	1.00	X
T_{air}	-	-	-	-	-	-	+0.103	-	+0.188	-	-	-	-0.376	-0.168	1.00
Pr	-	-0.128	-	-0.127	-	-	-	-	-0.123	+0.132	-	-	-	+0.269	-0.188

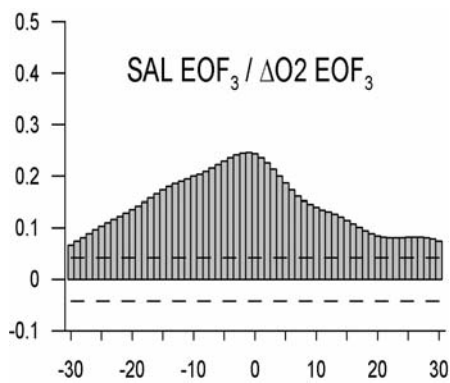


Figure 11. Time-lagged correlation between temporal variation of the "discharge" EOF modes of SAL and ΔO_2 .

sonal amplitude is aided by the non-linear dependence of oxygen on salinity; the mixing of oxygen-saturated freshwaters and oxygen-saturated saltwater results in a supersaturated mixture.

The seasonality of SST in the inshore areas is about two weeks ahead of the deeper offshore zones (Figure 6a). The explanation is that, over shallow areas, the response of SST to heat fluxes is more rapid and coincides better with the seasonal cycle of air temperature (see Figure 2e). In the deeper offshore zones, the seasonal cycle of SST lags that of air temperature by a couple of weeks.

The time of the seasonal minimum of surface salinity (Figure 6b) in SMB depends on freshwater

discharge from the two main sources of freshwater: Ballona Creek and the Hyperion Treatment Plant outfall. The freshwater discharge from Ballona Creek is directly related to atmospheric precipitation (Ackerman and Weisberg 2003). The seasonal minimum of SAL near Marina Del Rey occurs in late winter (end of January–early February) when precipitation is maximal (Figure 2f). In contrast, freshwater discharge from the Hyperion Treatment Plant does not exhibit significant seasonal variation (Eganhouse and Venkatesan 1993); yet there is a marked earlier onset of the seasonal SAL minimum directly above the outfall (Figure 6). This can be understood by the fact that the fraction of the effluent outflow that reaches the surface depends on the vertical stratification. During mid-winter, when vertical stratification is lowest and vertical mixing is highest (Winant and Bratkovich 1981), the highest fraction of freshwater discharged from the Hyperion outfall reaches the sea surface.

The phasing of the seasonal cycle in ΔO_2 in SMB generally shows a propagation from the south to the north. We interpret this trend as being driven mainly by an earlier onset of water column stratification in the southern parts of the Bay, which leads to a slightly earlier start of the phytoplankton bloom in winter/spring. A second interpretation is that winter/spring upwelling in SMB occurs preferentially along the northern shore (Gruber *et al.* in preparation). The upwelling brings oxygen-deficient waters to the surface. As long as upwelling is active, any net

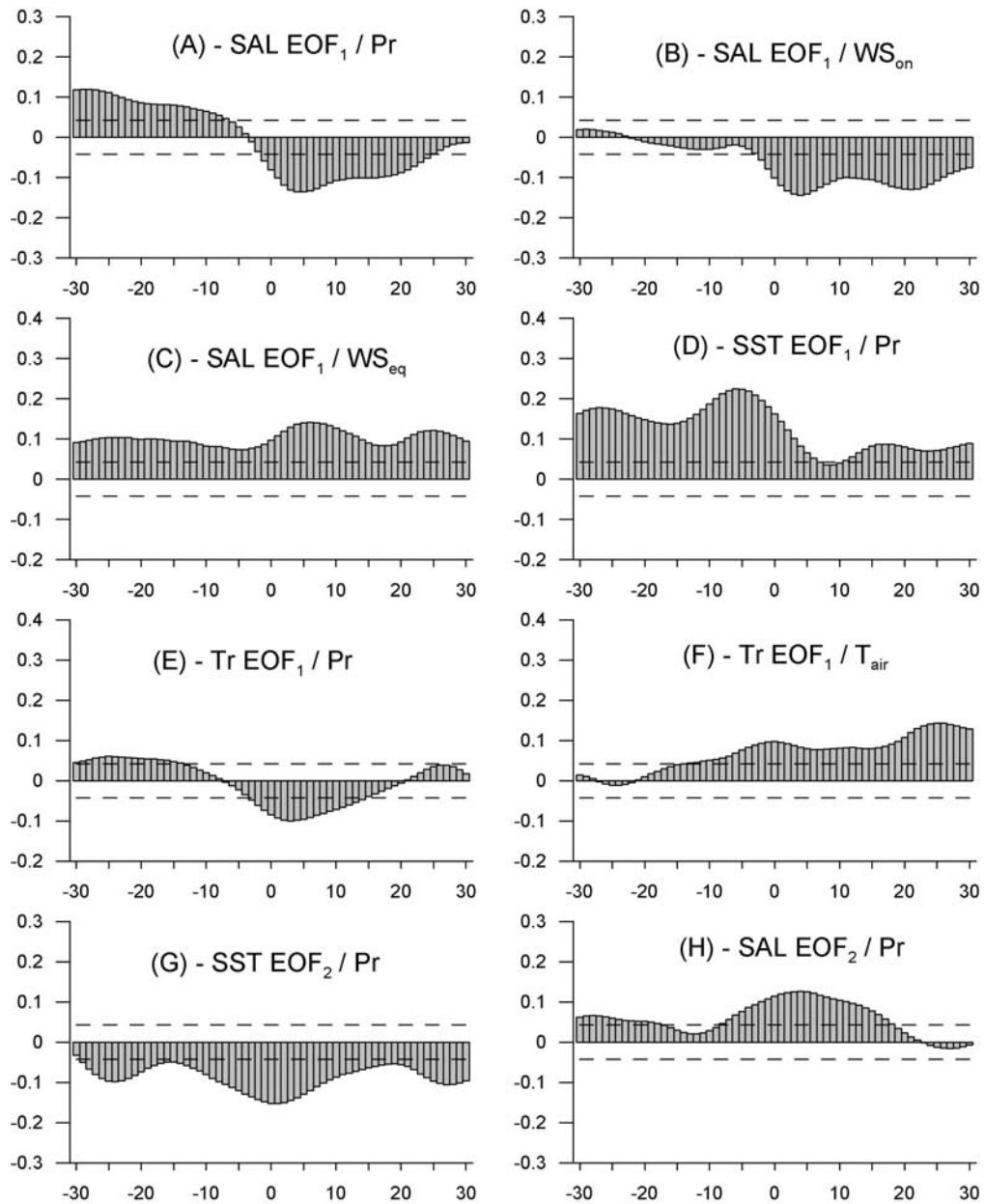


Figure 12. Time-lagged correlation between the time series of the principal components of EOF-1 (onshore/offshore mode) and EOF-2 (north/south mode) with various local meteorological parameters. Only those correlations are shown that are significant. (a) correlation as a function of lag between EOF-1 of salinity and precipitation; (b), as (a) but for onshore wind stress; (c), as (a) but for equatorward wind stress; (d) time-lag correlation between EOF-2 of SST and precipitation; (e) time-lag correlation between EOF-1 of %T and precipitation; (f), as (e) but for air temperature; (g) time-lag correlation between EOF-2 of SST and precipitation; (h) time-lag correlation between EOF-2 of salinity and precipitation.

Table 8. Coefficients of linear correlation between the external forcing WS_{eq} , WS_{on} , T_{air} , Pr and NINO3, averaged over SMB variables (SST, SAL, ΔO_2 , and %T), and the three leading EOF modes of SST (SST-1, SST-2, SST-3), SAL (SAL-1, SAL-2, SAL-3), ΔO_2 (ΔO_2 -1, ΔO_2 -2, ΔO_2 -3), %T (%T-1, %T-2, %T-3) after smoothing by 100 d linear filter.

	WS_{eq}	WS_{on}	T_{air}	Pr	NINO3
WS_{eq}	1.00	X	X	X	X
WS_{on}	-0.46	1.00	X	X	X
T_{air}	-0.47	+0.24	1.00	X	X
Pr	-0.17	+0.47	-0.06	1.00	X
NINO3	-0.43	+0.32	+0.45	+0.09	1.00
SST	-0.49	+0.40	+0.83	+0.04	+0.56
SAL	+0.60	-0.47	-0.17	-0.42	-0.29
ΔO	+0.15	+0.07	0.00	-0.47	+0.01
%T	+0.26	-0.17	+0.09	-0.23	-0.14
SST-1	-0.03	+0.06	-0.10	+0.44	-0.18
SST-2	+0.14	-0.07	+0.12	-0.33	-0.10
SST-3	+0.40	-0.47	-0.43	-0.08	-0.63
SAL-1	+0.47	-0.24	-0.11	+0.01	-0.21
SAL-2	+0.07	-0.25	-0.18	+0.14	-0.28
SAL-3	+0.19	+0.10	0.00	-0.03	-0.24
ΔO_{2-1}	-0.09	+0.15	+0.26	+0.03	+0.10
ΔO_{2-2}	-0.09	+0.41	+0.22	+0.18	+0.16
ΔO_{2-3}	+0.20	+0.08	-0.08	+0.04	-0.17
%T-1	+0.16	+0.16	+0.31	+0.04	+0.11
%T-2	+0.36	-0.18	-0.14	-0.12	-0.04
%T-3	-0.27	+0.13	+0.31	-0.02	+0.03

growth of phytoplankton is transported offshore; hence, phytoplankton concentration and ΔO_2 remain low along the northern shore. Only after upwelling relaxes can a phytoplankton bloom develop (Barber and Smith 1981).

The seasonal phasing of surface transmissivity matches the general pattern of SCB bottom topography. In shallow areas, seasonal extremes occur up to two months earlier than in the deeper zones (Santa Monica Canyon in the north of SMB and Redondo Canyon in the south). In the offshore zone of SMB, the seasonal minimum of transmissivity in mid-spring is a result of the spring bloom of phytoplankton, which occurs typically near the end of February (Nezlin and Li 2003). In the nearshore zones, the seasonal minimum of %T occurs closer to the time of the seasonal minimum of salinity in February, indicating that the input of suspended material from small rivers and creeks dominates the seasonal phasing there.

The succession of the seasonal extremes of the meteorological factors (T_{air} , Pr, WS_{eq} , and WS_{on}) illustrates the general cycles of these parameters in subtropical coastal areas. The dynamics of sea surface temperature is regulated by the balance of heat fluxes from above and cooling from below, resulting

from vertical mixing. The high heat capacity of the ocean relative to that of the air leads to a trailing of SST relative to air temperature; that is why the seasonal cycles of air temperature and SST trail the insolation cycle by about 1.5 and 2 months, respectively (Tont 1975).

Sub-seasonal variability: Sub-seasonal variations of the EOF modes

Despite the fact that the four oceanographic properties were analyzed independently, the results of the decomposition of each signal into orthogonal functions are remarkably similar. The first EOF modes of SST, SAL, ΔO_2 , and %T indicate inshore/offshore contrasts in oceanographic properties; the second EOF modes are related to the balance between the two main sources of horizontal advection into SMB; and the third EOF modes reveal the influence of freshwater discharge from Ballona Creek. However, the correlations between the same EOFs of the different properties are generally low. This indicates that the same modes for the different properties are not necessarily dynamically linked to each other despite their very similar spatial structure.

The spatial structure of the “inshore/offshore” mode has many similarities to the spatial structure of the seasonal amplitude. We suspect that the same processes responsible for generating the spatial structure of the seasonal amplitude are responsible for this sub-seasonal mode. The basic processes responsible for these correlations are the loss and gain of vertical stratification, resulting mostly from the heating and cooling of the sea surface. This process is most effective in the shallow near-shore zone. The decrease in ΔO_2 is counterintuitive, as one would expect an increase in ΔO_2 due to the warming. We suspect that the small warming effect is overwhelmed by a substantial decrease in the photosynthetic activity of the phytoplankton, which is the result of a reduction in the supply of nutrients into the upper layers caused by the increased stratification.

The positive correlations between temperature, salinity, and water transparency also indicate that the inshore/offshore EOF modes are likely related to the intensity of near-shore mixing. An intensive mixing inshore results in cool, desalinated, and turbid water; an enrichment of the surface layer with nutrients results in phytoplankton growth, which in turn causes an increase of ΔO_2 . It is worth mentioning that the highest correlation (+0.344) is observed between the

inshore/offshore modes of SAL and %T. We suppose that rain storms contribute to the inshore/offshore modes of salinity and transmissivity.

The correlation and pattern of the north/south EOF modes suggest that they are related to the balance between the two main sources of horizontal advection to SMB: one is the near-shore branch of the California Current flowing into SMB from the northwest (low temperature and salinity, high oxygen, and low transparency) and the other is the Southern California Countercurrent flowing in from the south (high temperature and salinity, low oxygen, and high transparency). The positive correlation between %T, and ΔO_2 in this north/south mode can be attributed to higher productivity of the California Current waters compared to the waters of the Southern California Countercurrent, as documented previously on the basis of large-scale observations (Chelton *et al.* 1982) and remotely sensed data by Coastal Zone Color Scanner (Pelaez and McGowan 1986, Smith *et al.* 1988, Thomas and Strub 1990) and by Sea-viewing Wide Field-of-view Sensor (SeaWiFS) radiometers (Nezlin *et al.* 2003).

As the name suggests, the correlations of the “discharge” modes can be traced back to the impact of freshwater discharges into SMB. The discharge of freshwater not only causes salinity to decrease, but is most likely the cause of the observed decrease of water transparency and increase in ΔO_2 . We suspect that the latter two changes are caused in part by enhanced productivity, which is driven by the freshwater derived input of nutrients. An additional reason for the high ΔO_2 values is the mixing of freshwaters with salty waters, which can cause supersaturation because of the non-linearity of the salinity dependence of the oxygen saturation concentration. A couple of weeks after each event of freshwater discharge (i.e., rainstorms), the oxygen concentration in this zone decreases. We attribute this change to a lowered biological productivity as well as to an increase in oxygen demand from the decay of the organic matter produced earlier, *in situ*, or swept by river runoff into SMB.

Sub-seasonal variability: Influence of local meteorological forcing on the SMB

An understanding of the correlation between air temperature, wind, and atmospheric precipitation is necessary to assess the correlations between oceano-

graphic properties and local meteorological factors (see Tables 5 and 7). Significant correlations exist between equatorward and onshore wind stresses (-0.23), between equatorward wind stress and air temperature (-0.38), between the onshore wind stress and precipitation (+0.27), and between air temperature and precipitation (-0.19). The first correlation simply indicates that wind stress is either predominantly perpendicular to the shore (i.e., from the southwest) or aligned with the shore (i.e., from the northwest). The second correlation is assumed to be a result of the fact that meridional winds are generally associated with a substantial heat transport by the atmosphere, leading to cool temperatures when the wind is from the north and vice versa. The correlation between on-shore transport and precipitation is likely caused by the transport of moist air masses from the sea toward the land, causing increased precipitation with increased moisture transport (Mo and Higgins 1998). The correlation between air temperature and precipitation simply suggests that rainy days are cooler on average.

High correlation between precipitation and salinity indicates freshwater discharge as a main source of salinity variations in SMB. The most pronounced decrease of salinity in SMB (about -2 psu) was observed in January 1993 (Figure 7b) and coincided with heavy rains (Figure 7d). Precipitation was the main source of variability of ΔO_2 and %T (see Table 5); i.e., freshwater discharge decreased both oxygen concentration and water transparency.

Atmospheric precipitation is negatively correlated with the inshore/offshore EOF mode of salinity. The time lag between these variations ranges from 0 to 20 d, with a maximum of about 4 to 5 d (Figure 12a). The rationalization of this correlation is straightforward, as each rainstorm results in a freshwater discharge to SMB, causing a decrease of salinity in the near-shore zone, while the changes in the offshore regions remain small. This signal is detected over a period of two to three weeks after each event. Precipitation exerts a similar but weaker influence on the transparency in the near-shore zone (Figure 12e). An increase in turbidity in the nearshore environment is very typical after a rain event. We suspect that the correlation between the inshore/offshore EOF mode of salinity and onshore wind stress (Figure 12b) results from the correlation between onshore wind and precipitation, rather than a direct influence.

The absence of a significant correlation between all three EOF modes of SST and air temperature in SMB on sub-seasonal timescales is worth discussing. This and the significant correlation between T_{air} and SST averaged over SMB (Table 5) suggest that variations of these modes on sub-seasonal timescales must be determined by large-scale processes rather than local coupling.

The variations of air temperature are correlated with the inshore/offshore mode of %T with a time lag of about one month (Figure 12f). This correlation can be explained by warm weather enhancing stratification of the upper mixed layer, which, in turn, inhibits both water mixing and phytoplankton growth, leading to an increase in water transparency. The time lag of one month suggests that biological processes (phytoplankton growth) might dominate over physical processes (turbidity resulting from suspension of bottom sediments).

Significant correlations exist between the equatorward and onshore wind stresses and the onshore/offshore EOF mode of salinity (Table 7; Figure 12b, c). These correlations exist over a wide range of time lags. This relationship coupled with a very weak correlation between the equatorward wind stress and SST (Table 5) is somewhat surprising, since one would expect that a stronger than usual equatorward wind stress would lead to upwelling and hence cooler than normal SSTs. However, as shown by Gruber *et al.* (in prep), wind conditions in SMB are too weak during most of the year to cause any significant upwelling. Secondly, the vertical stratification is too strong during most of the year to upwell waters that have distinctly colder temperatures and elevated nutrient levels. Only late winter/early spring storms that occur during a time of minimal vertical stability appear to cause any significant upwelling in SMB. As these events tend to be episodic, they do not show up in our correlation analyses.

Summarizing the analysis of the impact of local meteorological forcing on the sub-seasonal variations in SMB, we conclude that except for T_{air} /SST relation, and to some extent salinity and transmissivity, local meteorological forcing explains only a small fraction of the subseasonal variability. We suspect that internal ocean dynamics associated with the passage of eddies and other meso- and submeso-scale phenomena explain most of the remaining sub-seasonal variability. On longer timescales, large-scale forcing by the atmosphere and ocean, such as induced, for example, by northward propagating

coastally trapped waves associated with ENSO events in the Tropical Pacific, might have a distinct influence on SMB variability as well.

Intraseasonal to interannual variability

The signs and magnitudes of the interannual anomaly correlations between the equatorward wind stress, SST, and SAL clearly point toward upwelling being the cause of these correlations. An increase in the equatorward wind stress enhances the offshore Ekman transport and hence upwelling. As upwelling occurs in SMB primarily in winter and spring, when salinity tends to increase with depth, the cooler than normal SSTs induced by the upwelling are accompanied by higher salinities. Although not significant, years with elevated upwelling also tend to have higher oxygen supersaturations and more turbid waters. We suspect that the correlations between the onshore wind stress and SST and SAL are similarly driven by upwelling processes, but occurring at locations where the large-scale onshore wind stress is aligned with some part of the coastline.

SST and air temperature are even more correlated on interannual timescales than they are on sub-seasonal timescales. This suggests that SST in SMB is closely coupled to large-scale forcing. This is particularly evident by the high correlation of SST with the NINO3 index. A negative correlation emerges between SAL and NINO3, which is expected, as the positive phases of ENSO (El Niño) are known to increase precipitation in Southern California quite substantially (Ropelewski and Halpert 1986, Haston and Michaelsen 1994). The strong forcing of interannual anomalies of SST and SAL within SMB by the tropical Pacific is remarkable and merits further discussion.

During the warm phase of ENSO (El Niño), the eastward propagating equatorial Kelvin waves that are generated in the western Pacific (Wyrtki 1975, McPhaden *et al.* 1990, Kessler and McPhaden 1995, Chavez *et al.* 1999, McPhaden 1999) are transformed at the South American coast into coastally trapped waves. These waves propagate north and south along the west coast of the Americas toward the poles (Enfield and Allen 1980, Chelton and Davis 1982, Huyer and Smith 1985), deepening the thermocline and raising sea level along the coast. The resulting accumulation of warm water in the upper ocean results in large positive sea surface temperature anomalies. The redistribution of SST over the Pacific Ocean changes atmospheric circulation, reflected, for example, in an expansion of the

Aleutian Low (Emery and Hamilton 1985). Some scientists consider the influence of ENSO on the local atmospheric circulation (“atmospheric teleconnection”) to be the main source of the changes in the hydrography and ecology of the California Current system (Simpson 1983, 1984a, 1984b, Mysak 1986, Breaker and Lewis 1988, Breaker *et al.* 2001, Schwing *et al.* 2002); other researchers emphasize the direct influence of the coastal waves (Huyer and Smith 1985, Rienecker and Mooers 1986, Lynn *et al.* 1995, Chavez 1996, Ramp *et al.* 1997, Schwing *et al.* 2002).

El Niño events were especially pronounced during our observations (1987–1997), because the period from 1976 to 1998 belongs to a warm phase of the Pacific Decadal Oscillation (PDO) (Smith 1995). In 1998–1999, the warm PDO phase abruptly changed to a cold phase (Bograd *et al.* 2000, Bograd and Lynn 2003, Chavez *et al.* 2003, McGowan *et al.* 2003). The warm phase of PDO, like ENSO, tends to bring warmer winter temperatures to the Pacific Northwest, whereas the cool phase produces La Niña-like cooler winter conditions (Mantua *et al.* 1997, Zhang *et al.* 1997, Chao *et al.* 2000). PDO modulates ENSO teleconnections through constructive or destructive ENSO-PDO phase pairings. In constructive or “in-phase” relationships, El Niño signals tend to be strong and stable during a warm PDO phase and La Niña signals tend to be strong and stable during a cool PDO phase. On the other hand, in destructive or “out-of-phase” pairings (warm PDO/La Niña and cool PDO/El Niño), ENSO signals tend to be weak and unstable (Gershunov and Barnett 1998).

Inspection of the NINO3 index in Figure 10e shows that the beginning of our observations in 1987 coincided with an El Niño event, followed by a La Niña in 1988. The next El Niño was observed in 1991–1992; it was rather smooth and was not followed by a La Niña. Both events had a substantial effect on the West Coast of North America (Lenarz *et al.* 1995, Lynn *et al.* 1995, Mullin 1995, Murphree and Reynolds 1995, Chavez 1996). The end of our observations coincided with the onset of the 1997–1998 El Niño event, the strongest in the twentieth century (Chavez *et al.* 1999, McPhaden 1999).

The time for the coastally trapped waves to propagate northward from the equatorial Pacific is two months or less (Fiedler 1984, Spillane *et al.* 1987, Kosro 2002). If these waves were the only external factor driving interannual anomalies in SMB, one would expect a maximum in the correlation between

NINO3 and properties within SMB at such a time lag. As it turns out, the time-lag correlation between SST in SMB and NINO3 is quite broad with a maximum at time-lag zero, suggesting that a combination of atmospheric teleconnection and coastal wave dynamics is responsible for the SST anomalies. Another factor to consider is that our smoothing with a 100-d filter tends to suppress correlations shorter than this period.

A substantial negative correlation is observed between the NINO3 index and the SST EOF modes. Taking into account the correlations between NINO3 and WS_{eq} , WS_{on} , and T_{air} , this negative correlation indicates a “flattening” of the SST pattern in SMB during the El Niño events resulting from a combination of remote and local forcings.

Significant correlations between the wind stress and the “north/south” ΔO_2 and %T EOF modes indicate the influence of dominant winds on the contrast between these properties of the water transported to SMB from the northwest and from the south. This influence is related to phytoplankton growth rather than to the hydrographical variables. We speculate that wind stress influences upwelling located not in SMB but elsewhere (probably to the northwest in Santa Barbara Channel and further), and the resulting “biological signal” is transported to SMB by the horizontal flow.

Some extremes in the time series of the EOF modes can be explained by the extremes of the external forcing; these relations are often not reflected in the correlation coefficients. For example, the inshore/offshore SST EOF mode was not correlated with air temperature, wind, and NINO3 index. At the same time, its first minimum in January 1988 and the subsequent maximum in March 1988 (Figure 9a) are related to the simultaneous variations of air temperature anomalies (Figure 10c) and can be attributed to local variations in ocean/atmosphere heat flux. The next minimum of the inshore/offshore SST EOF mode in July 1988 was very strong, but not related to local meteorological factors. However, it coincided with the onset of the 1988 La Niña event (Kerr 1988) (Figure 10e). The shallow zone of SMB appeared to be most sensitive to remote forcing from the tropical Pacific, as compared with its deeper part. The next substantial minimum of the inshore/offshore SST EOF mode occurred in June 1989 (Figure 9a). It coincides with well-pronounced maximum of the equatorward wind stress (i.e., the offshore upwelling index) anomaly (Figure 10a). We consider

this event a manifestation of coastal upwelling, resulting in cooling of the SMB nearshore zone. The next minimum of the inshore/offshore SST EOF mode was observed in September 1989; it coincided with a local minimum of air temperature and should be attributed to local ocean/atmosphere interactions.

A substantial maximum of the inshore/offshore SST EOF mode was observed in July–September 1990; it coincided with the decrease of the equatorward wind stress. We speculate that this event could be an example of coastal downwelling resulting from southerly winds; a similar situation was documented earlier by Winant (1980)

The maximum of the inshore/offshore SST EOF mode in February 1991 and the minima in June–July 1991, May 1994, and April–May 1995 coincided with the negative anomalies of air temperature. We attribute the positive anomaly of the inshore/offshore SST EOF mode in August–September 1991 to the onset of the 1991 El Niño event shown in Figure 10e.

High values of the inshore/offshore SST EOF mode were observed during the winter seasons of 1994–95, 1995–96, and 1996–97. These periods were characterized by high values of the onshore wind stress (Schwing *et al.* 1997, see also Figure 10b) resulting in strengthening of the equatorward alongshore flow transporting cold water of the California Current to SMB from the northwest. This cold upwelled water retained in a deep part of SMB, in turn, increased the contrast between sea surface temperature in the nearshore and offshore parts of SMB.

Schwing *et al.* (1997) called the period from late 1995 until early 1997 “a weak La Niña.” There was a strong transition in atmospheric circulation between the fall of 1994 and winter/spring 1995, resulting in anomalous southerly/southwesterly winds along the west coast of the United States (Hayward *et al.* 1995). The decrease of equatorward wind stress is also evident from Figure 10a. The southerly wind caused onshore water transport and was associated with severe ecological consequences, including torrential rains (see Figure 10d) and a red tide event (the bloom of dinoflagellate *Gonyaulax polyedra* Stein) during January–April 1995 in a wide inshore area of the Southern California Bight, including SMB (Hayward *et al.* 1995). The bloom reached concentrations of more than 2 million cells L⁻¹. A substantial decrease of the inshore/offshore gradients of oxygen anomalies and turbidity during

the first half of 1995 are likely caused by this red tide (Figures 9e, g).

LITERATURE CITED

- Ackerman, D. and S.B. Weisberg. 2003. Relationship between rainfall and beach bacterial concentrations on Santa Monica Bay beaches. *Journal of Water and Health* 1: 85-89.
- Bakun, A. 1973. Coastal upwelling indices, west coast of North America, 1946–1971. NOAA Technical Report NMFS SSRF-671. U.S. Department of Commerce. Washington, DC.
- Bakun, A. and C.S. Nelson. 1991. The seasonal cycle of wind-stress curl in subtropical eastern boundary current regions. *Journal of Physical Oceanography* 21: 1815-1834.
- Barber, R.T. and R.L. Smith. 1981. Coastal upwelling ecosystems. pp. 31-68 in: A.R. Longhurst (ed.), *Analysis of Marine Ecosystems*. Academic Press. London, England.
- Bograd, S.J., P.M. DiGiacomo, R. Durazo, T.L. Hayward, K.D. Hyrenbach, R.J. Lynn, A.W. Mantyla, F.B. Schwing, W.J. Sydeman, T. Baumgartner, B. Lavaniegos, and C. S. Moore. 2000. The state of the California Current, 1999–2000: Forward to a new regime? *California Cooperative Oceanic Fisheries Investigations Reports* 41: 26-52.
- Bograd, S.J. and R.J. Lynn. 2003. Long-term variability in the Southern California Current System. *Deep-Sea Research* 50: 2355-2370.
- Bray, N.A., A. Keyes and W.M.L. Morawitz. 1999. The California Current system in the Southern California Bight and the Santa Barbara Channel. *Journal of Geophysical Research* 104: 7695-7714.
- Breaker, L.C. and P.A. W. Lewis. 1988. A 40-50 day oscillation in sea-surface temperature along the central California coast. *Estuarine, Coastal and Shelf Science* 26: 395-408.
- Breaker, L.C., P.C. Liu and C. Torrence. 2001. Intraseasonal oscillations in sea surface temperature, wind stress, and sea level off the central California coast. *Continental Shelf Research* 21: 727-750.
- Broecker, W.S. and T.-H. Peng. 1974. Gas exchange rates between air and sea. *Tellus*, 26: 21-35.
- Chao, Y., M. Ghil and J.C. McWilliams. 2000. Pacific interdecadal variability in this century sea surface temperatures. *Geophysical Research Letters* 27: 2261-2264.

- Chavez, F.P. 1996. Forcing and biological impact of onset of the 1992 El Niño in central California. *Geophysical Research Letters* 23: 265-268.
- Chavez, F.P., J. Ryan, S.E. Lluch-Cota and M.C. Niquen. 2003. From anchovies to sardines and back: Multidecadal change in the Pacific Ocean. *Science* 299: 217-221.
- Chavez, F.P., P.G. Strutton, G.E. Friedrich, R.A. Feely, G.C. Feldman, D.G. Foley and M.J. McPhaden. 1999. Biological and chemical response of the equatorial Pacific Ocean to the 1997-98 El Niño. *Science* 286: 2126-2131.
- Chelton, D.B., P.A. Bernal and J.A. McGowan. 1982. Large-scale interannual physical and biological interaction in the California Current. *Journal of Marine Research* 40: 1095-1125.
- Chelton, D.B. and R.E. Davis. 1982. Monthly mean sea-level variability along the west coast of North America. *Journal of Physical Oceanography* 12: 757-784.
- Dalkey, A. and J.F. Shisko. 1996. Observations of oceanic processes and water quality following seven years of CTD surveys in Santa Monica Bay, California. *Bulletin of the Southern California Academy of Sciences* 95: 17-32.
- DiGiacomo, P.M. and B. Holt. 2001. Satellite observations of small coastal ocean eddies in the Southern California Bight. *Journal of Geophysical Research* 106: 22521-22543.
- Dorman, C.E. and C.D. Winant. 1995. Buoy observations of the atmosphere along the west coast of the United States. *Journal of Geophysical Research* 100: 16029-16044.
- Dorman, C.M. and D.P. Palmer. 1981. Southern California summer coastal upwelling. pp. 44-56 in: F. A. Richards (ed.), Coastal Upwelling. American Geophysical Union. Washington, DC.
- Dwight, R.H., J.C. Semenza, D.B. Baker and B.H. Olson. 2002. Association of urban runoff with coastal water quality in Orange County, California. *Water Environment Research* 74: 82-90.
- Eganhouse, R.P. and M.I. Venkatesan. 1993. Chemical oceanography and geochemistry. pp. 71-189 in: M.D. Dailey, D.J. Reish and J.W. Anderson (eds.), Ecology of the Southern California Bight. University of California Press. Berkeley, CA.
- Emery, K.O. 1960. The Sea off Southern California. John Wiley & Sons, Inc. New York, NY.
- Emery, W.J. and K. Hamilton. 1985. Atmospheric forcing of interannual variability in the northeast Pacific Ocean, connections with El Niño. *Journal of Geophysical Research* 90: 857-868.
- Enfield, D.B. and J.S. Allen. 1980. On the structure and dynamics of monthly mean sea level anomalies along the Pacific coast of North and South America. *Journal of Physical Oceanography* 10: 557-578.
- Eppley, R.W. and E.H. Renger. 1988. Nanomolar increase in surface layer nitrate concentration following a small wind event. *Deep-Sea Research* 35: 1119-1125.
- Eppley, R.W., E.H. Renger and W.G. Harrison. 1979. Nitrate and phytoplankton production in the southern California coastal waters. *Limnology and Oceanography* 24: 483-494.
- Fiedler, P.C. 1984. Satellite observations of the 1982-1983 El Niño along the U.S. Pacific Coast. *Science* 224: 1251-1254.
- Garcia, H.E. and L.I. Gordon. 1992. Oxygen solubility in seawater: Better fitting equation. *Limnology and Oceanography* 37: 1307-1312.
- Gershunov, A. and T.P. Barnett. 1998. Interdecadal modulation of ENSO teleconnections. *Bulletin of the American Meteorological Society* 79: 2715-2725.
- Gruber, N., H. Frenzel, W.M. Hamner, P. Marchesiello, J.C. McWilliams, N.P. Nezlin, J. Oram and K. Stolzenbach. In preparation. Biological-physical coupling during an upwelling event in Santa Monica Bay, CA. *Journal of Geophysical Research*.
- Halpern, D. (ed.). 2000. Satellites, Oceanography and Society. (Vol. 63). Elsevier. Amsterdam, The Netherlands.
- Haston, L. and J. Michaelsen. 1994. Long-term central coastal California precipitation variability and relationship to El Niño-Southern Oscillation. *Journal of Climate* 7: 1373-1387.
- Hayward, T.L., D.R. Cayan, P.J.S. Franks, R.J. Lynn, A.W. Mantyla, J.A. McGowan, P.E. Smith, F.B. Schwing and E.L. Venrick. 1995. The state of the California Current in 1994-1995: A period of transition. *California Cooperative Oceanic Fisheries Investigations Reports* 36: 19-39.
- Hickey, B.M. 1979. The California Current system: Hypotheses and facts. *Progress in Oceanography* 8: 191-279.

- Hickey, B.M. 1992. Circulation over the Santa Monica-San Pedro basin and shelf. *Progress in Oceanography* 30: 37-115.
- Hickey, B.M. 1993. Physical oceanography. pp. 19-70 in: M.D. Dailey, D.J. Reish and J.W. Anderson (eds.), *Ecology of the Southern California Bight*. University of California Press. Berkeley, CA.
- Hickey, B.M., E.L. Dobbins and S.E. Allen. 2003. Local and remote forcing of currents and temperature in the central Southern California Bight. *Journal of Geophysical Research* 108: 3081, doi:10.1029/2000JC000313.
- Huyer, A. and R.L. Smith. 1985. The signature of El Niño off Oregon in 1982-83. *Journal of Geophysical Research* 90: 7133-7142.
- Isaaks, E.H. and R.M. Srivastava. 1989. *Applied Geostatistics*. Oxford University Press. New York, NY.
- Kerr, R.A. 1988. La Niña big chill replaces El Niño. *Science* 241: 1037-1038.
- Kessler, W.S. and M.J. McPhaden. 1995. The 1991-1993 El Niño in the central Pacific. *Deep-Sea Research II* 42: 295-333.
- Kosro, P.M. 2002. A poleward jet and an equatorward undercurrent observed off Oregon and northern California, during the 1997-98 El Niño. *Progress in Oceanography* 54: 343-360.
- Lenarz, W.H., D.A. Ventresca, W.M. Graham, F.B. Schwing and F. Chavez. 1995. Explorations of El Niño events and associated biological population dynamics off central California. *California Cooperative Oceanic Fisheries Investigations Reports* 36: 106-119.
- Lynn, R.J., F.B. Schwing and T.L. Hayward. 1995. The effect of the 1991-1993 ENSO on the California Current system. *California Cooperative Oceanic Fisheries Investigations Reports* 36: 57-71.
- Lynn, R.J. and J.J. Simpson. 1987. The California Current System: The seasonal variability of its physical characteristics. *Journal of Geophysical Research* 92: 12947-12966.
- Mantua, N.J., S.R. Hare, Y. Zhang, J.M. Wallace and R.C. Francis. 1997. A Pacific Interdecadal Climate Oscillation with impacts on salmon production. *Bulletin of the American Meteorological Society* 78: 1069-1079.
- McGowan, J.A., S.J. Bograd, R.J. Lynn and A.J. Miller. 2003. The biological response to the 1977 regime shift in the California Current. *Deep-Sea Research II* 50: 2567-2582.
- McPhaden, M.J. 1999. Genesis and evolution of the 1997-98 El Niño. *Science* 283: 950-954.
- McPhaden, M.J., S.P. Hayes, L.J. Mangum and J.M. Toole. 1990. Variability of the western equatorial Pacific Ocean during 1986-87 El Niño/Southern Oscillation event. *Journal of Physical Oceanography* 20: 190-208.
- Mo, K.C. and R.W. Higgins. 1998. Tropical influences on California precipitation. *Journal of Climate* 11: 412-430.
- Mullin, M.M. 1995. The Californian El Niño of 1992 and the fall of Calanus. *California Cooperative Oceanic Fisheries Investigations Reports* 36: 175-178.
- Murphree, T. and C. Reynolds. 1995. El Niño and La Niña effects on the northeast Pacific: The 1991-1993 and 1988-1989 events. *California Cooperative Oceanic Fisheries Investigations Reports* 36: 45-56.
- Mysak, L.A. 1986. El Niño, interannual variability and fisheries in the northeast Pacific Ocean. *Canadian Journal of Fisheries and Aquatic Sciences* 43: 464-497.
- Nezlin, N.P., W.M. Hamner and L.D. Zeidberg. 2003. Remote-sensed analysis of the influence of 1997-1998 El Niño on the California pelagic ecosystem. pp. 284-301 in: S. B. Weisberg (ed.), *Southern California Coastal Water Research Project Annual Report 2001-2002*. Southern California Coastal Water Research Project Authority. Westminster, CA.
- Nezlin, N.P. and B.-L. Li. 2003. Time-series analysis of remote-sensed chlorophyll and environmental factors in the Santa Monica-San Pedro Basin off Southern California. *Journal of Marine Systems* 39: 185-202.
- Oliver, M.A. and R. Webster. 1990. Kriging: A method of interpolation for geographical information system. *International Journal of Geographical Information Systems* 4: 313-332.
- Pelaez, J. and J.A. McGowan. 1986. Phytoplankton pigment patterns in the California Current as determined by satellite. *Limnology and Oceanography* 31: 927-950.
- Priesendorfer, R.W. 1988. *Principle Component Analysis in Meteorology and Oceanography*. Elsevier Science. New York, NY.
- Raco-Rands, V.E. and A. Steinberger. 2001. Characteristics of effluents from large municipal wastewater treatment facilities in 1997. pp.28-44 in: S.B. Weisberg (ed.), *Southern California Coastal Water Research Project Annual Report 1999-2000*. Southern California Coastal Water Research Project Authority. Westminster, CA.

- Ramp, S.R., J.L. McClean, C.A. Collins, A.J. Semtner and K.A.S. Hays. 1997. Observations and modeling of the 1991-1992 El Niño signal off central California. *Journal of Geophysical Research* 102: 5553-5582.
- Rienecker, M.M. and C.N.K. Mooers. 1986. The 1982-1983 El Niño signal off northern California. *Journal of Geophysical Research* 91: 6597-6608.
- Ropelewski, C.F. and M.S. Halpert. 1986. North American precipitation and temperature patterns associated with the El Niño/Southern Oscillation (ENSO). *Monthly Weather Review* 114: 2352-2362.
- Schwing, F.B., T.L. Hayward, K.M. Sakuma, T. Murphree, A.S. Mascarenhas, Jr., S.I.L. Castillo, A.W. Mantyla, S.L. Cummings, F.P. Chavez, K. Baltz and D.G. Ainley. 1997. The state of the California Current, 1996-1997: Mixed signals from the tropics. *California Cooperative Oceanic Fisheries Investigations Reports* 38: 22-47.
- Schwing, F.B., T. Murphree, L. deWitt and P.M. Green. 2002. The evolution of oceanic and atmospheric anomalies in the northeast Pacific during the El Niño and La Niña events of 1995-2001. *Progress in Oceanography* 54: 459-491.
- Simpson, J.J. 1983. Large-scale thermal anomalies in the California Current during the 1982-1983 El Niño. *Geophysical Research Letters* 10: 937-940.
- Simpson, J.J. 1984a. El Niño-induced onshore transport in the California current during 1982-1983. *Geophysical Research Letters* 11: 241-242.
- Simpson, J.J. 1984b. A simple model of the 1982-1983 Californian "El Nino". *Geophysical Research Letters* 11: 243-246.
- Smith, P.E. 1995. A warm decade in the Southern California Bight. *California Cooperative Oceanic Fisheries Investigations Reports* 36: 120-126.
- Smith, R.C., X. Zhang and J. Michaelsen. 1988. Variability of pigment biomass in the California Current System as determined by satellite imagery. 1. Spatial variability. *Journal of Geophysical Research* 93: 10863-10882.
- Spillane, M.C., D.B. Enfield and J.S. Allen. 1987. Intraseasonal oscillations in sea level along the west coast of the Americas. *Journal of Physical Oceanography* 17: 313-325.
- Sverdrup, H.U. and R.H. Fleming. 1941. The waters off the coast of southern California, March to July 1937. *Bulletin of the Scripps Institution of Oceanography* 4: 261-378.
- Thomas, A.C. and P.T. Strub. 1990. Seasonal and interannual variability of pigment concentrations across a California Current frontal zone. *Journal of Geophysical Research* 95: 13023-13042.
- Tont, S.A. 1975. The effect of upwelling on solar irradiance near the coast of Southern California. *Journal of Geophysical Research* 80: 5031-5034.
- Winant, C.D. 1980. Downwelling over the Southern California shelf. *Journal of Physical Oceanography* 10: 791-799.
- Winant, C.D. and A.W. Bratkovich. 1981. Temperature and currents on the southern California shelf: A description of the variability. *Journal of Physical Oceanography* 11: 71-86.
- Wyrtki, K. 1975. Fluctuations of the dynamic topography in the Pacific Ocean. *Journal of Physical Oceanography* 5: 450-459.
- Zhang, Y., J.M. Wallace and D.S. Battisti. 1997. ENSO-like interdecadal variability: 1900-93. *Journal of Climate* 10: 1004-1020.

ACKNOWLEDGEMENTS

We are indebted to A. Dalkey for making the hydrographic observations available to us and to all the people who collected and analyzed the data. We thank W.M. Hamner, S. Weisberg, E. Stein, S. Bograd, M. Mengel, A. Dalkey, and an unknown reviewer for critical discussion of the results. This study was supported by California Seagrant (#R/CZ-171), the University of California Coastal Environmental Quality Initiative Program, the U.S. National Science Foundation, and the National Aeronautics and Space Administration.